

# 1 **Active synthesis of collagen (I) homotrimer and matrisomal proteins in** 2 **Dupuytren's fibrosis**

3  
4 Kate Williamson<sup>a</sup>, Katie J. Lee<sup>a</sup>, Emma L. Beamish<sup>a</sup>, Deborah Simpson<sup>b</sup>, Alan Carter<sup>a</sup>, Jade A. Gumbs<sup>a,c</sup>,  
5 Graham Cheung<sup>d</sup>, Daniel Brown<sup>a,d</sup>, Rob Pettitt<sup>e</sup>, Eithne J. Comerford<sup>a,c,e</sup>, Peter D. Clegg<sup>a,c</sup>, Elizabeth G.  
6 Canty-Laird<sup>a,c,\*</sup>

7  
8 \* Corresponding author (elizabeth.laird@liverpool.ac.uk)

9  
10 <sup>a</sup> Department of Musculoskeletal and Ageing Science, Institute of Life Course and Medical Sciences, University  
11 of Liverpool, William Henry Duncan Building, 6 West Derby Street, Liverpool, L7 8TX, United Kingdom

12 <sup>b</sup> Technology Directorate, Centre for Proteome Research, Department of Biochemistry & Systems Biology,  
13 Institute of Systems, Molecular & Integrative Biology, University of Liverpool, Crown Street, Liverpool L69  
14 7ZB

15 <sup>c</sup> The Medical Research Council Versus Arthritis Centre for Integrated Research into Musculoskeletal Ageing  
16 (CIMA)

17 <sup>d</sup> Liverpool University Hospitals NHS Foundation Trust, Liverpool, United Kingdom

18 <sup>e</sup> Institute of Infection, Veterinary and Ecological Sciences, Leahurst Campus, University of Liverpool, Chester  
19 High Road, Neston, CH64 7TE, United Kingdom

## 20 21 **Abstract**

22 Dupuytren's disease is a common fibroproliferative disease of the palmar fascia of the hand with severe  
23 cases treated surgically. The rate of disease recurrence following treatment is high and a continual  
24 production of matrisomal proteins could lead to disease recurrence. There is no animal model for  
25 Dupuytren's disease, but analysis of the surgically excised tissue provides an accessible means to study the  
26 mechanisms of human tissue fibrosis. Here we sought to determine how new synthesis and the  
27 composition of matrisomal proteins in Dupuytren's differs from normal palmar fascia samples, using  
28 metabolic labelling approaches and proteomics. Model non-fibrotic, but fibrous connective tissues, equine  
29 flexor tendon and canine cranial cruciate ligament, were used to analyse active collagen-1 protein synthesis  
30 in development, ageing and degenerative disease, where it was restricted to early development and  
31 ruptured tissue. Dupuytren's tissue was shown to actively synthesise type I collagen, a proportion of which  
32 comprised abnormal collagen (I) homotrimer (mean 14.3% ± 14.4), as well as fibronectin, matrix  
33 metalloproteinases (MMP2, MMP3) and their inhibitors; Tissue Inhibitor of Metalloproteinases 2 (TIMP2).  
34 Insulin-Like Growth Factor Binding Protein 7 (IGFBP7) was actively synthesised by Dupuytren's as well as  
35 control tissue. Label-free analysis implicated the TGFβ pathway in the matrisomal profile of Dupuytren's  
36 tissue whilst myocilin, a Wnt-pathway regulator, was noticeably more abundant in control samples. No  
37 collagen (I) neopeptides representing the major collagenase cleavage site were identified, however  
38 periostin neopeptides were abundant in Dupuytren's tissue and gelatin neopeptides in both tissue types.  
39 Synthesis of MMP-resistant collagen-1 homotrimer, together with altered TGFβ and Wnt signalling  
40 environments, could contribute to the persistence of the fibrotic tissue and disease recurrence following  
41 treatment.

42  
43

## 44 Introduction

45

46 Fibrillar collagens, particularly type I, are the major structural component of fibrous connective tissue  
47 including palmar fascia (aponeurosis), tendon, ligament, and fibrotic tissue. In fibrous tissue string-like  
48 fibrils comprise arrays of collagen molecules. Excessive accumulation of fibrillar collagens impedes normal  
49 tissue function resulting in particularly poor outcomes in cardiac, pulmonary, kidney and liver fibrosis  
50 (Wynn, 2008; Zeisberg and Kalluri, 2013). Dupuytren's disease is a common fibroproliferative disorder of  
51 the palmar fascia of the hand, which has sex, age, geographic and racial differences; being most prevalent  
52 in, but not restricted to, older men of Northern European descent (Hindocha et al., 2009). The aetiology of  
53 Dupuytren's is similarly complex involving genetics; an autosomal dominance pattern with varying  
54 penetrance, links to other diseases such as diabetes, epilepsy and liver disease, and environmental factors  
55 including alcohol intake and smoking (Grazina et al., 2019).

56 The formation of fibrous tissue under the skin can cause of Dupuytren's patients can cause  
57 localised pain and discomfort whilst disease progression may prevent the digits from straightening,  
58 producing fixed flexion contractures. The disease severity is commonly measured by the degree of joint  
59 contraction (which can be monitored Tubiana staging), the number of digits involved and the presence of  
60 disease outside the hand; Ledderhose disease in the foot or Peyronie's disease in the penis (Dibenedetti et  
61 al., 2011; Hindocha et al., 2008).

62 Treatment options include surgery; fasciectomy (excising the diseased tissue) and  
63 dermofasciectomy (excising the disease tissue and overlying skin), percutaneous needle aponeurotomy  
64 (dividing the diseased tissue) and did include collagenase treatment (prior to withdrawal from several  
65 jurisdictions) (Soreide et al., 2018); with each treatment carrying varying success, complications and  
66 recurrence rates (Krefter et al., 2017). In patients with advanced disease and debilitating contractures, the  
67 gold standard treatment is open limited fasciectomy followed by physiotherapy to encourage range of  
68 movement (Worrell, 2012). Surgical complication rates increase with disease severity and range between 3-  
69 50% (Craxford and Russell, 2016), whilst recurrence in the same finger/thumb or disease progression in  
70 other digits is common (8-54%) (Worrell, 2012).

71 The fibrotic tissue in Dupuytren's can comprise a highly cellular 'nodule' region, which is thought to  
72 represent an active stage in the tissue pathogenesis and a 'cord' region, consisting of mature fibrillar  
73 collagen (Layton and Nanchahal, 2019). Disease pathogenesis has been divided into proliferative,  
74 involutinal (contracting) and residual stages, with progressively decreasing cellularity and increasing  
75 alignment along directional lines of tension (Luck, 1959). Type III collagen is present at very low levels in  
76 normal palmar fascia, but is abundant in Dupuytren's tissue (Brickley-Parsons et al., 1981). However, the  
77 proportion of type III collagen relative to total collagen decreases through the stages of disease progression  
78 from >35% to <20% in the residual stage (Lam et al., 2010). Myofibroblasts are abundant in nodules, display  
79 persistent alpha-smooth muscle actin (alpha-SMA) expression and are responsible for both matrix  
80 deposition and contraction. Bidirectional actin-fibronectin interactions (Tomasek and Haaksma, 1991)  
81 result in the progressive tensioning of collagen fibres and a concurrent increase in total flexion deformity  
82 (Verjee et al., 2009). Other cell types implicated in the initiation or progression of Dupuytren's fibrosis  
83 include embryonic stem cells, mesenchymal stromal cells, fibrocytes and immune cell populations (Layton  
84 and Nanchahal, 2019; Tan et al., 2018).

85 A systematic review of Dupuytren's disease 'omics' studies highlighted alterations in collagen and  
86 extracellular matrix (ECM) gene expression as well as genomic and transcriptomic studies implicating the  
87 TGF $\beta$  and Wnt signalling pathways in disease pathogenesis (Shih et al., 2012). One study has utilised  
88 proteomics in Dupuytren's disease and a two-dimensional gel electrophoresis approach implicated  
89 activation of the Akt signalling pathway as well as alterations in cytoskeletal proteins and those involved in

90 extracellular and intracellular signalling, oxidative stress and cellular metabolism (Kraljevic Pavelic et al.,  
91 2009).

92 Analysis of messenger RNA (mRNA) expression profiles in isolated Dupuytren's fibroblasts found  
93 increased collagen and ECM mRNAs (Forrester et al., 2013), whilst a loss of collagen-regulating microRNAs  
94 (miRs) was identified in Dupuytren's tissue (Riester et al., 2015). A weighted gene co-expression network  
95 analysis and functional enrichment analysis of Dupuytren's transcriptomic datasets found gene ontology  
96 terms for ECM and collagen in ECM organisation, ECM-receptor interaction and collagen catabolic process,  
97 as well as adhesion and endoplasmic reticulum (ER) stress terms (Jung et al., 2019). An altered expression  
98 of matrix metalloproteinases (MMPs) has also been identified in Dupuytren's disease, as well as of a  
99 disintegrin and metalloproteinase domain with thrombospondin motif proteins (ADAMTSs) and tissue  
100 inhibitors of metalloproteinases (TIMPs), (Forrester et al., 2013; Johnston et al., 2007) whilst MMP14  
101 variants are genetically linked to Dupuytren's (Ng et al., 2017).

102 Type I collagen molecules are predominantly  $(\alpha 1)_2(\alpha 2)_1$  heterotrimers derived from the polypeptide  
103 gene products of the *COL1A1* and *COL1A2* genes. However, abnormal collagen  $(\alpha 1)_3$  homotrimer has been  
104 identified in Dupuytren's tissue (Ehrlich et al., 1982). Collagen (I) homotrimers are resistant to  
105 MMP-mediated proteolytic degradation (Makareeva et al., 2010) and may therefore skew the balance  
106 between collagen (I) synthesis and degradation, impeding the resolution of fibrosis.

107 We hypothesised that there may be a continual production of abnormal homotrimeric type I  
108 collagen or an altered profile of ECM that could contribute to the recurrence of Dupuytren's contracture  
109 following medical treatment. In this study, we utilised metabolic labelling approaches in combination with  
110 1D gel electrophoresis or proteomics to analyse type I collagen and global protein synthesis and  
111 degradation in fibrotic Dupuytren's tissue, and in non-fibrotic but fibrous connective tissue. The study  
112 aimed to determine how new and residual fibrotic ECM differs from that produced in normal fibrous tissue  
113 and how collagen-1 synthesis differs from that seen in development, or tissue injury, with a view to  
114 identifying specific ECM proteins or pathways as targets for future anti-fibrotic therapy.

115  
116

## 117 **Methods**

118

### 119 **Sample collection**

120 After full informed written consent (REC13/NW/0352 and REC 14/NW/0162 ), excised Dupuytren's tissue  
121 (fibrotic palmar fascia) and control non-diseased normal palmar fascia (PF), were taken from human  
122 patients undergoing surgery, at the Royal Liverpool and Broadgreen University Hospitals NHS Trust (now  
123 Liverpool University Hospitals NHS Foundation Trust) or the Warrington and Halton Hospitals NHS  
124 Foundation Trust (now Warrington and Halton Teaching Hospitals NHS Foundation Trust), for Dupuytren's  
125 contracture and Carpal tunnel syndrome respectively. Self-reported demographics were collected by  
126 questionnaire, and for the Dupuytren's patients disease stage information was collected from clinical  
127 records. Equine superficial digital flexor tendon (SDFT) and healthy canine cranial cruciate ligament (CCL)  
128 were collected as described (Ali et al., 2018; Lee et al., 2018), with local ethical approval (VREC186, VREC62  
129 and RETH00000553). Ruptured CCL, otherwise discarded as clinical waste, was obtained from dogs  
130 undergoing stifle/knee stabilisation at the University of Liverpool's Small Animal Teaching Hospital  
131 (VREC63). Surgical samples were reserved in cold sterile saline and processed on the day of collection  
132 according to the selected analysis method.

133  
134  
135

## 136 Quantitative real-time PCR (qPCR)

137 Tissue samples were immersed in RNAlater (Qiagen) and stored at -20°C until analysis. The tissue was  
138 homogenised with a mikrodismembrator or a pestle and mortar in 1 ml of TRI Reagent® (Sigma-Aldrich,  
139 Poole, UK). 0.1 ml 1-bromo-3-chloropropane (BCP) (Sigma-Aldrich) was added to the homogenate and  
140 centrifuged for 15 minutes at 12,000 x g at 4°C. 1 µg of total RNA was reverse transcribed with M-MLV  
141 reverse transcriptase using random primers according to the manufacturer's protocol (Promega). RT-qPCR  
142 was performed in a 25 µl reaction volume containing; complementary DNA (cDNA) (5 ng), primers designed  
143 for the gene of interest (Table 1) and GoTaq(R) qPCR Master Mix (Promega). Samples were run on an AB  
144 7300 Real Time PCR System (Applied Biosystems) using the following amplification conditions; 2 minutes at  
145 95°C followed by 40 cycles of 15 seconds at 95°C and 1 minute at 60°C. Gene expression was calculated  
146 relative to GAPDH, which was determined to be a suitable reference gene after assessing its stability using  
147 the geNorm method.

148

149 **Table 1: Primer Sequences**

Species	Gene	Forward	Reverse
Human	COL1A1	GTTCAGCTTTGTGGACCTCCG	GATTGGTGGGATGTCTTCGTCT
	COL1A2	AGCCGGAGATAGAGGACCAC	AGCAAAGTCCCACCGAGAC
	GAPDH	ATGGGGAAGGTGAAGGTCG	TAAAAGCAGCCCTGGTGACC
Equine	COL1A1	CATGTTCAGCTTTGTGGACCT	TGACTGCTGGGATGTCTTCTT
	COL1A2	CATGTTCAGCTTTGTGGACCT	TTTCCTGCAGTTGCCTCTTGT
	GAPDH	GCATCGTGGAGGGACTCA	GCCACATCTCCCAGAGG
Canine	COL1A1	CCAGCCGCAAAGAGTCTACAT	TGACTGGTGGGATGTCTTCT
	COL1A2	ACAAGGAGTCTGCATGTCTAAGT	GCAGTTGCCTCCTGTAAAGA
	GAPDH	CTGGGGCTCACTTGAAAGG	CAAACATGGGGGCATCAG

150

151

## 152 Pulse-chase with <sup>14</sup>C-L-proline

153 Tissue samples were aseptically dissected into pieces, with an estimated wet weight of 25-50 mg or volume  
154 of ~25-50 µL each, under PBS or Dulbecco's minimal essential medium (DMEM), containing  
155 penicillin/streptomycin (1% v/v). After a 30-60 minute pre-equilibration at 37°C in DMEM containing  
156 penicillin/streptomycin (1% v/v), L-glutamine (2 mM), L-ascorbic acid 2-phosphate (200 µM) and β-  
157 aminopropionitrile (400 µM) (labelling media) with ~1-5 pieces per 1 ml of media, pulse-chase experiments  
158 were performed in labelling media supplemented with 2.5 µCi/ml [<sup>14</sup>C]proline (GE Healthcare). After  
159 incubation in supplemented labelling media for 18 hrs, tissue samples were transferred to labelling media  
160 without [<sup>14</sup>C]proline for 3 hrs. Subsequently, 1-2 tissue pieces were extracted in 100 µl aliquots of salt  
161 extraction buffer (1 M NaCl, 25 mM EDTA, 50 mM Tris-HCl, pH 7.4) containing protease inhibitors. Extracts  
162 were analysed by electrophoresis on 6% Tris-Glycine gels (ThermoFisher) with delayed reduction (Sykes et  
163 al., 1976) or on 4% Tris-Glycine gels (Invitrogen, discontinued) under reducing conditions. The gels were  
164 fixed in 10% methanol, 10% acetic acid, dried under vacuum, and exposed to a phosphorimaging plate  
165 (BAS-IP MS). Phosphorimaging plates were processed using a phosphorimager (Typhoon FLA7000 IP) and  
166 densitometry carried out using ImageQuant (GE Healthcare Life Sciences). The α1(I):α2(I) chain ratio was  
167 converted to a percentage homotrimeric collagen using the formula; (ratio-2)x100/ratio.

168

169

## 170 **Metabolic labelling with $^{13}\text{C}_6$ -L-lysine and mass spectrometry**

171 Dupuytren's and normal palmar fascia dissections were performed aseptically under DMEM containing  
172 penicillin/streptomycin (1% v/v). Dupuytren's samples were dissected into cord and nodule regions after  
173 removal of any surrounding fatty tissue, and then cut into pieces with an estimated wet weight of 25-50 mg  
174 or volume of ~25-50  $\mu\text{L}$  each. Normal PF samples were cut into two approximately equal sized pieces of a  
175 similar size. For each sample type, 1-2 tissue pieces were equilibrated in 1ml complete unlabelled SILAC  
176 media for 30 minutes at 37°C 5%  $\text{CO}_2$  and then in 1ml complete [ $^{13}\text{C}_6$ ]L-lysine labelled SILAC media (Lee et  
177 al., 2019) for 18-24 hours. Explants were then weighed, snap frozen and stored at -80°C whilst incubation  
178 medium was stored in aliquots at -20°C.

179 Tissue samples were disrupted using a Mikro-Dismembrator (Braun International) under liquid  
180 nitrogen. Approximately 10 mg of tissue was weighed directly into LoBind tubes (Eppendorf), snap frozen  
181 and stored at -80°C. For prior chondroitinase treatment, 80  $\mu\text{l}$  of Chondroitinase ABC (AMSBIO AMS.E1028-  
182 10) at 1 U/ml in 100mM Tris Acetate containing protease inhibitors with EDTA was used per 10 mg of  
183 homogenized tissue and the chondroitinase supernatant reserved. A sequential GnHCl followed by 0.1%  
184 RapiGest extraction was carried out as described by (Ashraf Kharaz et al., 2017), except that 100  $\mu\text{l}$  of  
185 GnHCl extraction buffer containing 1 mM EDTA was used per 10mg of starting material, the subsequent  
186 steps scaled similarly and the final Rapigest pellet extraction not carried out. For tissue extracts and  
187 chondroitinase supernatants filter-aided sample preparation (FASP) was carried out with centrifugation  
188 steps at 12,500 rpm for 15 minutes unless otherwise indicated. 100  $\mu\text{l}$  of formic acid (1% v/v) was added to  
189 each filter (Vivacon 500, 10,000 MWCO, Sartorius) and spun. Extract from an equivalent of 2 mg of tissue or  
190 the entire chondroitinase supernatant was added to each filter and made up to 200  $\mu\text{l}$  with 4M GnHCl in  
191 50mM ammonium bicarbonate (GnHCl buffer). A 15-minute incubation in 8mM DTT in GnHCl buffer at 56°C  
192 in the dark with gentle vortexing preceded a 10-minute spin. Each filter was washed twice with 100  $\mu\text{l}$  4M  
193 GnHCl buffer and spun. 100  $\mu\text{l}$  of 50mM iodoacetamide in GnHCl buffer was used to alkylate proteins with  
194 gentle vortexing and a 20-minute incubation in the dark before a 10-minute spin. Each filter was washed  
195 twice with 100ul GnHCl buffer, then thrice with 50mM ammonium bicarbonate with a 10-minute spin.  
196 Bound proteins were digested with 40  $\mu\text{l}$  of trypsin at 10ng/ $\mu\text{l}$  in 47.5mM ammonium bicarbonate with  
197 2.5mM acetic acid at 37°C overnight with steps to prevent evaporation, followed by a 10-minute spin and a  
198 subsequent wash with 40  $\mu\text{l}$  of 50mM ammonium bicarbonate. Combined flow-throughs were acidified  
199 with Trifluoroacetic acid to 0.2% (v/v). Incubation media was bound to and digested off Strataclean beads  
200 as previously described (Angi et al., 2016; Ashraf Kharaz et al., 2017). A yeast enolase peptide standard was  
201 added to each sample, though this was not utilised for later quantification. Liquid chromatography tandem  
202 mass spectrometry (LC-MS/MS) was carried out as described (Lee et al., 2019) with loading volumes  
203 determined from prior ranging runs.

## 205 **Proteomic data analysis**

206 Protein identification, label-free quantification and analysis of  $^{13}\text{C}_6$ -L-lysine labelling was carried out as  
207 described (Lee et al., 2019) with the following modifications. *De novo* and database PEAKS searches were  
208 carried out using the UniHuman database with Waters Pepmix. Fragment mass error tolerance was set to  
209 0.02 Da in searches and Proteins  $-10\text{lgP} \geq 20$  in filters. Results were normalized to the equivalent wet  
210 weight of tissue loaded on the trapping column or using the total ion chromatogram (TIC) and analysed  
211 using PeaksQ (Peaks Studio v8, Bioinformatics Solutions, Waterloo, Canada). The Dupuytren's:Normal PF  
212 ratio for each protein was calculated from group profile ratios as (Nodule+Cord)/(Normal PF x 2), converted  
213 to an expression fold change in IPA (Ingenuity Pathway Analysis, Qiagen) and used therein for analysis of  
214 upstream regulators. The Dupuytren's:Normal PF ratio was used to define proteins associated with each

215 tissue type for which protein interactions and pathways were analysed using STRING (Szklarczyk et al.,  
216 2019) using default settings.

217 Neopeptide analysis was carried out as described by (Peffer et al., 2014) with the following  
218 modifications. The UniHuman database was used and search parameters were enzyme; semiTrypsin,  
219 fragment mass tolerance; 0.01 Da, peptide charge; 2+, monoisotopic, instrument; ESI-QUAD-TOF and decoy  
220 selected. Peptide modifications were fixed carbamidomethyl cysteine, variable oxidation of methionine and  
221 variable heavy ( $^{13}\text{C}_6$ ) lysine. Results were filtered for those neopeptides present in at least three normal PF  
222 samples or at least three cord and nodule samples

223

## 224 **Statistical analysis**

225 Data analysis was performed using SigmaPlot Version 14.0 and graphing carried out with GraphPad Prism 8  
226 for Windows (GraphPad Software, La Jolla California USA, [www.graphpad.com](http://www.graphpad.com)), unless otherwise indicated.  
227 Plots show individual data points together with the mean and +/- 1 SD unless otherwise indicated. COL1A1  
228 and COL1A2 gene expression data was analysed using a Mann-Whitney rank sum test, whilst  
229 COL1A1:COL1A2 ratios were analysed using a t-test. For Bayesian analysis of the donor ages of samples  
230 analysed by qRT-PCR and proteomics, a free online Bayes factor calculator was used  
231 ([http://www.lifesci.sussex.ac.uk/home/Zoltan\\_Dienes/inference/bayes\\_factor.swf](http://www.lifesci.sussex.ac.uk/home/Zoltan_Dienes/inference/bayes_factor.swf)) with a uniform age  
232 prior and upper and lower bounds of 75 and -75 respectively, to obtain a Bayes factor as described (Dienes,  
233 2014). Polypeptide chain ratios were analysed using a one-sample t-test.

234 Principal components analysis (PCA) and associated graphing was carried out using Minitab®  
235 Statistical Software Version 18 (State College, PA: Minitab, Inc. ([www.minitab.com](http://www.minitab.com))) as was Box-Cox data  
236 transformation. For PCA incorporating demographic data, self-reported textual data was coded in a binary  
237 manner except for diabetes - where diet-controlled (coded 1) was distinguished from type I (coded 2),  
238 smoking - where previous smokers were coded 1 and current smokers coded 2, alcohol consumption -  
239 where those consuming below the recommended limit were coded 1 and those above coded 2, and  
240 exercise - which was coded from 0-3 based on apparent intensity/duration.

241 For heavy lysine labelled peptides in media, a two-way ANOVA with tissue type and peptide as  
242 factors was used with a Holm-Sidak post-hoc test. Data failing the Shapiro-Wilk normality test and/or the  
243 Brown-Forsythe equal variance test was transformed using a Box-Cox transformation prior to analysis.  
244 Where a suitable transformation could not be found data were analysed using a Kruskal-Wallis one-way  
245 ANOVA on ranks with Dunn's pairwise comparisons.

246

247 **Results**

248

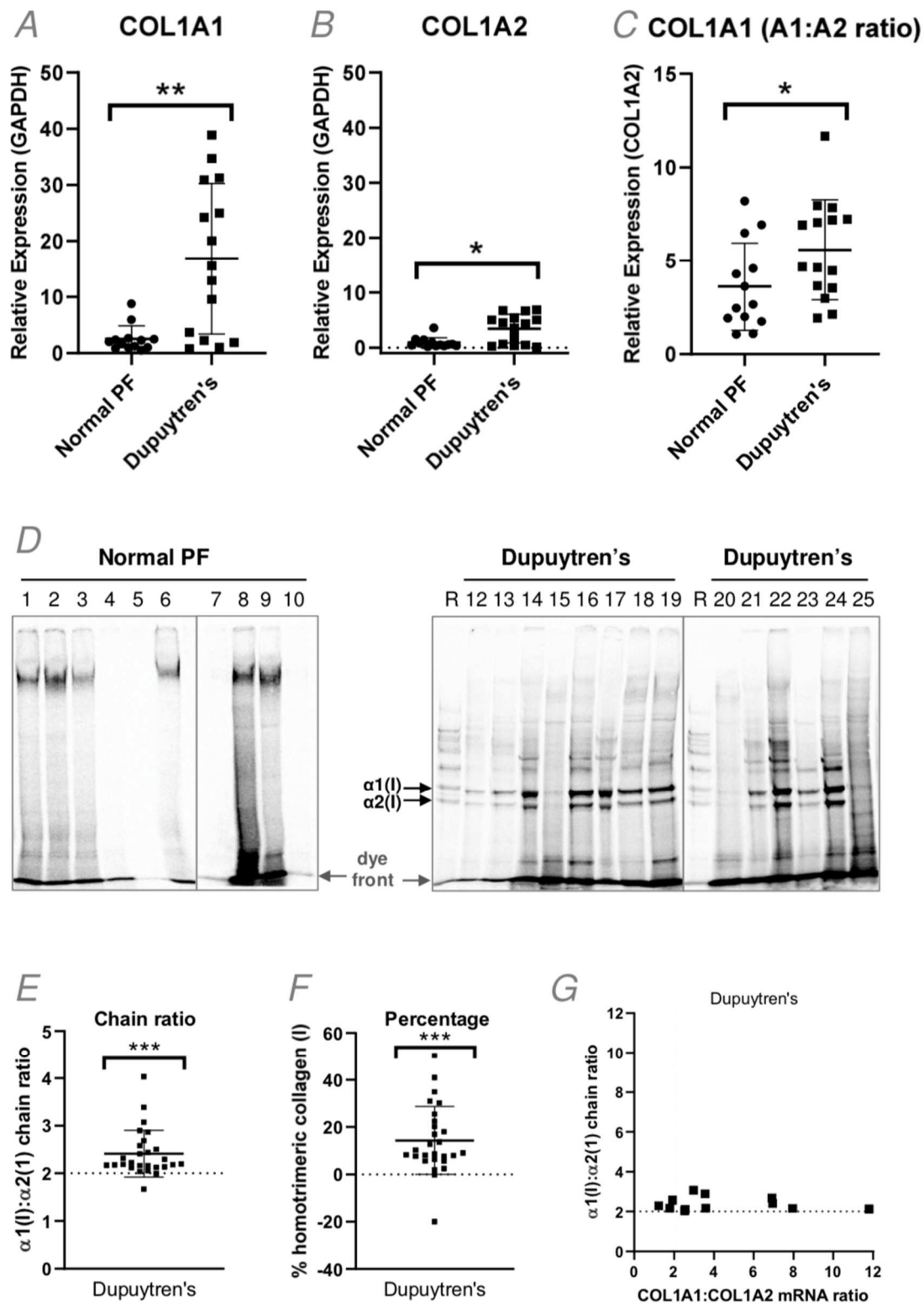
249 **Collagen (I) homotrimer is actively produced by Dupuytren's tissue**

250 To determine if collagen (I) homotrimer is continuously synthesized in Dupuytren's tissue, COL1A1 and  
251 COL1A2 gene expression was measured by qRT-PCR, and synthesis of  $\alpha$ -chains by radiolabelling, in  
252 Dupuytren's samples and in normal PF controls. Expression of COL1A1 (Fig. 1A) and COL1A2 (Fig. 1B) was  
253 significantly higher in Dupuytren's tissue, indicative of new collagen (I) synthesis. The relative expression of  
254 COL1A1 as compared to COL1A2 was also higher in Dupuytren's tissue (Fig. 1C) indicating increased gene  
255 transcription and/or mRNA stability of COL1A1 as compared to COL1A2. There was no significant difference  
256 in the age of the Dupuytren's and normal PF samples that were analysed by qRT-PCR ( $p=0.11$ ). A Bayesian  
257 analysis was used to determine if there was truly no difference in age between the groups, but results were  
258 inconclusive ( $B=0.34$ , insensitive).

259 Metabolic labelling with  $^{14}\text{C}$  proline indicated Dupuytren's tissue explants but not normal PF  
260 controls ( $n=22$ ) produced newly-synthesised collagen (I) protein (Fig. 1D). Samples derived from 27 of 31  
261 Dupuytren's patients were sufficiently labelled for densitometric quantification (Supplementary Results).  
262 The  $\alpha 1(\text{I}):\alpha 2(\text{I})$  chain ratio was significantly greater than 2 (Fig. 1E) indicative of new collagen (I)  
263 homotrimer synthesis. Using the ratios for the nodule only in the analyses (discounting 3 other cord  
264 samples) produced similar results (not shown). The  $\alpha 1(\text{I}):\alpha 2(\text{I})$  ratio was converted to a percentage of  
265 homotrimeric collagen (I), indicating a mean value of 14.3% ( $\text{SD} \pm 14.4\%$ ) and with one sample reading  
266 50.4% (Fig. 1F). Plotting the  $\alpha 1(\text{I}):\alpha 2(\text{I})$  ratio against the COL1A1:COL1A2 mRNA ratio indicated no direct  
267 correlation between relative mRNA and polypeptide chain ratios (Fig. 1G).

268

269



270

271

272

273

274

275

276

277

278

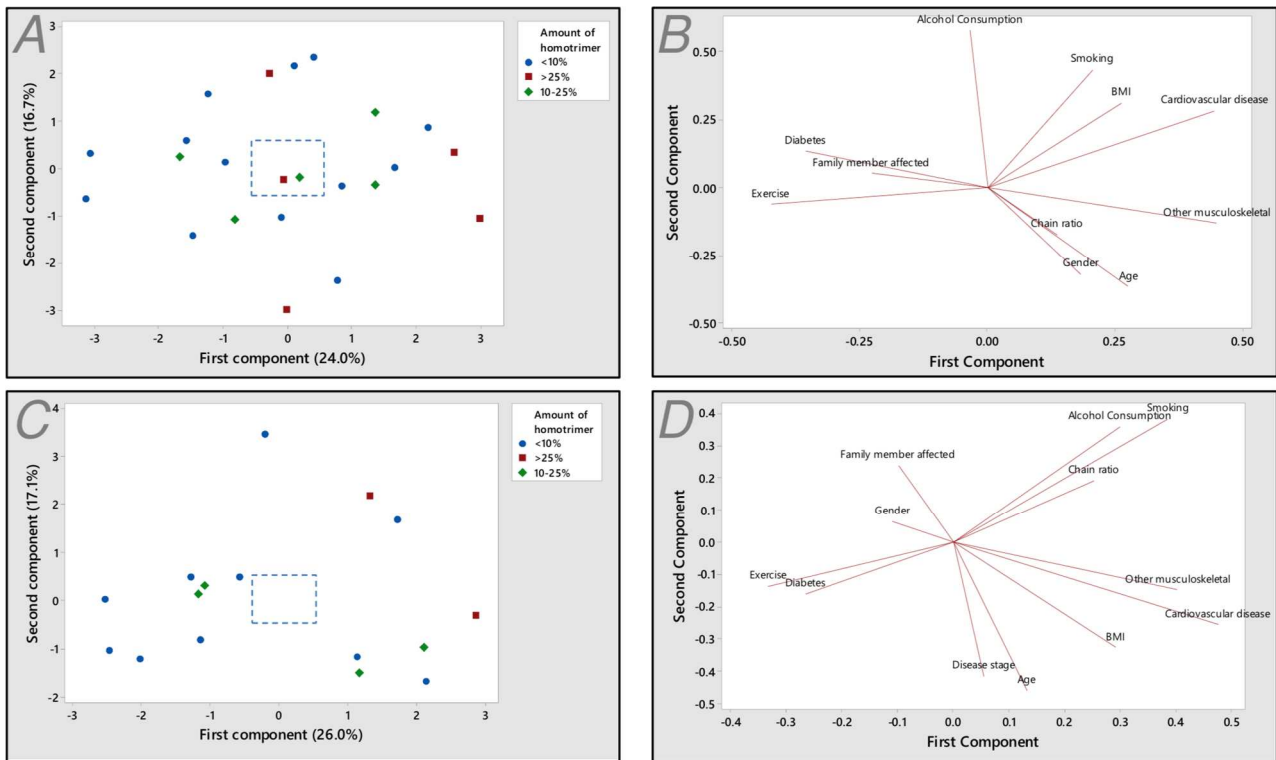
**Figure 1: Synthesis of type I collagen homotrimer by Dupuytren's tissue.** A-C: Analysis of COL1A1 (A), COL1A2 (B) and COL1A1:COL1A2 (C) gene expression by qRT-PCR in normal PF (n=13) and Dupuytren's tissue samples (n=15). D: Representative delayed reduction 6% SDS-Page gels of normal PF (D) and Dupuytren's (E) tissue extracts after pulse-chase labelling with [<sup>14</sup>C]proline. E-F: The relative amounts of the labelled  $\alpha 1(I)$  and  $\alpha 2(I)$  chains in Dupuytren's (n=27) samples were quantified by densitometry and expressed as an  $\alpha 1(I):\alpha 2(I)$  chain ratio (E) or converted to a percentage of homotrimeric type I collagen (I) (F). The  $\alpha 1(I):\alpha 2(I)$  chain ratio was plotted against the COL1A1:COL1A2 mRNA ratio for Dupuytren's samples (n=12) for which both data types were available (G). \* p < 0.05, \*\* p < 0.01 and \*\*\* p < 0.001.



279

## 280 Demographic factors are not associated with greater collagen (I) homotrimer synthesis

281 To determine if particular demographics factors were associated with an increased proportion of  
282 homotrimeric collagen (I), a PCA was carried out (Fig. 2). Samples producing lower (<10%), medium (10-  
283 25%) or higher (>25%) percentages of homotrimeric collagen (I) were not grouped based on demographics  
284 factors (Fig. 2A). Demographic loading (Fig. 2B) had a minimal effect on principal component scores. To  
285 determine whether disease stage influences collagen (I) homotrimer synthesis, the PCA was repeated on  
286 samples with paired disease stage, which also showed only a weak effect (Fig. 2C-D).  
287



288

289

290 **Figure 2: Principal components analysis of the relationship between demographic factors and the**  
291 **proportion of homotrimeric collagen.** A: Score plot grouped by lower (<10%), medium (10-25%) and  
292 higher (>25%) percentages of collagen (I) homotrimer (n=23). The box indicates the relative scale on the  
293 loading plot (B). C-D: Score plot (C) and loading plot (D) for a patient sub-set with disease stage information  
294 (n=16).  
295  
296  
297  
298  
299  
300  
301  
302  
303  
304  
305  
306

307 **Active type I collagen synthesis in diseased, ruptured or foetal, but not healthy adult fibrous**  
308 **connective tissue**

309 No radiolabelled normal PF samples were found to synthesise detectable amounts of type I collagen in  
310 explant culture, but a high molecular weight band was noted in 10 of the 22 labelled normal PF samples  
311 (examples shown in Fig. 1D). Under reducing conditions, a single band migrating similarly to the  $\alpha 2(I)$  chain  
312 was noted in normal PF samples and one between the  $\alpha 1(I)$  and  $\alpha 2(I)$  chain in some Dupuytren's samples  
313 (#s 12, 14 and 19) (Fig. 3A). The identity of the labelled proteins in these bands are unknown but are  
314 expected to be collagenous given the incorporation of labelled proline.

315 We considered that the age and normal status of the normal PF samples may preclude detectable  
316 levels of new type I collagen synthesis. Model non-fibrotic fibrous connective tissues were therefore  
317 studied. Analysis of canine cranial cruciate ligament (CCL) allowed a comparison between healthy fibrous  
318 tissue, and that ruptured due to degenerative disease, whilst analysis of equine superficial digital flexor  
319 tendon (SDFT) facilitated a comparison across ages: foetal, young, adult and old. The relative expression of  
320 both COL1A1 (Fig. 3B) and COL1A2 (Fig. 3C) was significantly increased in ruptured canine cranial cruciate  
321 ligament as compared to healthy samples. The expression of COL1A1 relative to COL1A2 was higher in  
322 ruptured ligament (Fig. 3D), although the ratio did not exceed 1.5. Ruptured ligament produced newly-  
323 synthesised type I collagen whilst under reducing conditions healthy ligament produced a single band  
324 migrating between the  $\alpha 1(I)$  and the  $\alpha 2(I)$  chain (Fig. 3E). Foetal SDFT produced nascent type I collagen as  
325 expected, whilst all post-natal SDFT samples did not; instead producing a band co-migrating with  $\alpha 2(I)$   
326 (similar to human normal PF), a higher molecular weight band co-migrating with pC $\alpha 2(I)$  and often a band  
327 migrating between pro $\alpha 1(I)$  and pC $\alpha 1(I)$ .

328

329

330

331

332

333

334

335

336

337

338

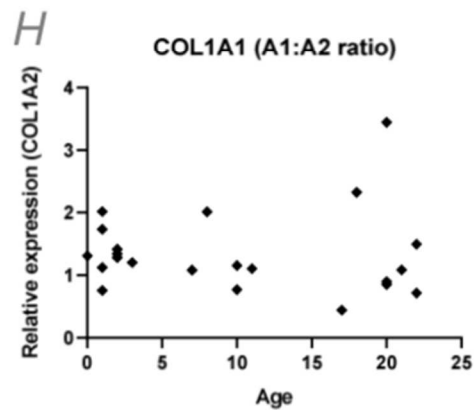
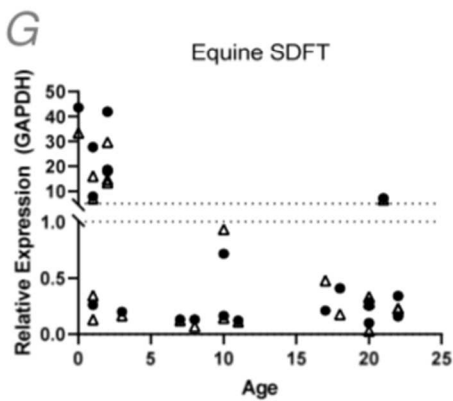
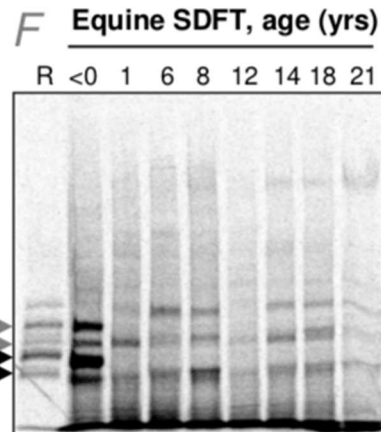
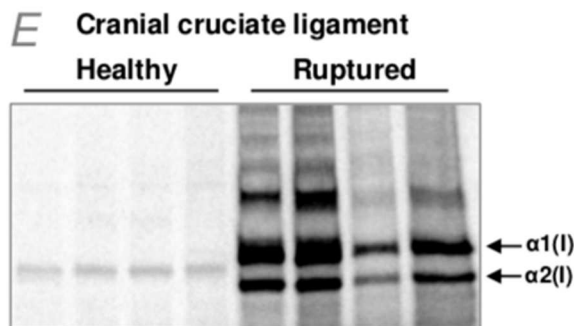
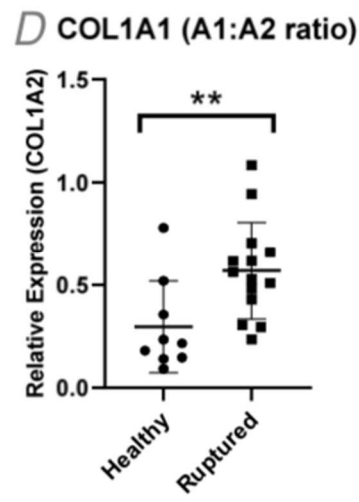
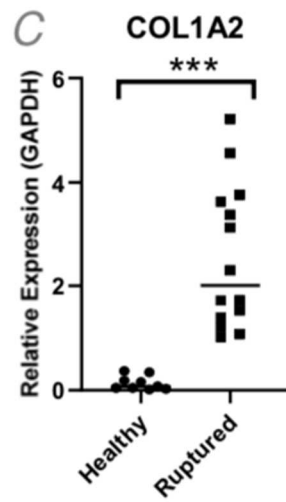
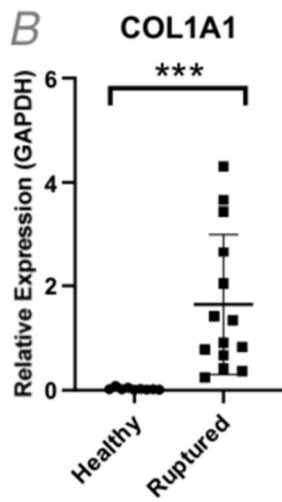
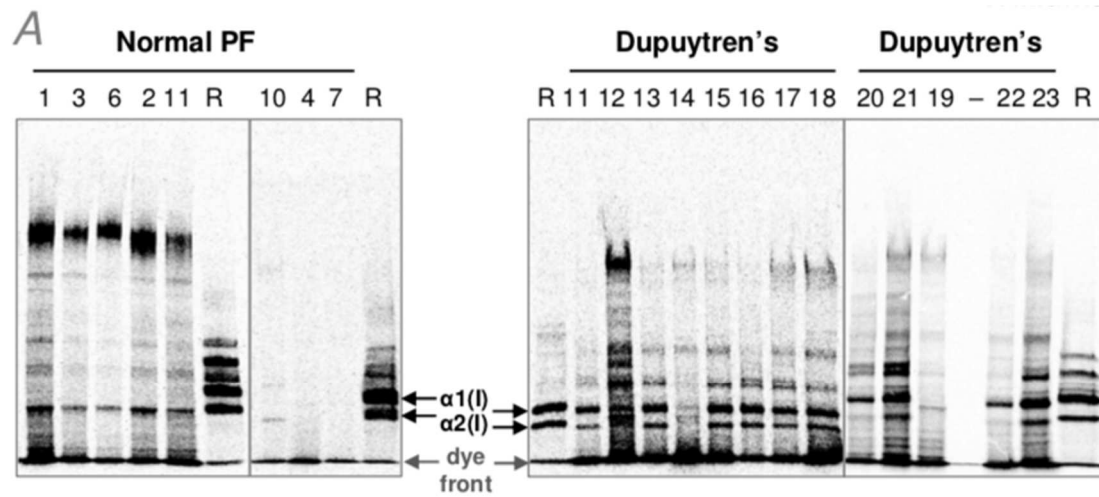
339

340 *Over page:*

341

342 **Figure 3: Type I collagen and proline-rich protein synthesis in tendon and ligament explants. A:**

343 Representative 4% SDS-Page gels of reduced normal PF and Dupuytren's tissue extracts after pulse-chase  
344 labelling with [ $^{14}C$ ]proline. Sample numbers relate to those shown in Figure 1D. B-D: Analysis of COL1A1 (B),  
345 COL1A2 (C) and COL1A1:COL1A2 (D) gene expression by qRT-PCR in healthy (n=9) and ruptured (n=14)  
346 canine cranial cruciate ligament samples. E: Representative 4% SDS-Page gel of reduced healthy and  
347 ruptured canine cranial cruciate ligament extracts after pulse-chase labelling with [ $^{14}C$ ]proline. F:  
348 Representative 4% SDS-Page gel of equine superficial digital flexor tendon (SDFT) extracts at different ages  
349 after pulse-chase labelling with [ $^{14}C$ ]proline. G-H: Analysis of COL1A1 and COL1A2 (G) and COL1A1:COL1A2  
350 (H) gene expression by qRT-PCR in equine superficial digital flexor tendon (SDFT) at various ages. Note  
351 horses have an average 25-30 year lifespan, with 20 years being equivalent to approximately 60 human  
352 years.



354  
355  
356  
357  
358  
359  
360  
361  
362  
  
363  
364  
365  
366  
367  
368  
369  
370  
371  
372  
373  
374  
375  
376  
377  
378  
379  
380  
381  
382

### Active synthesis of matrisomal proteins by Dupuytren's tissue

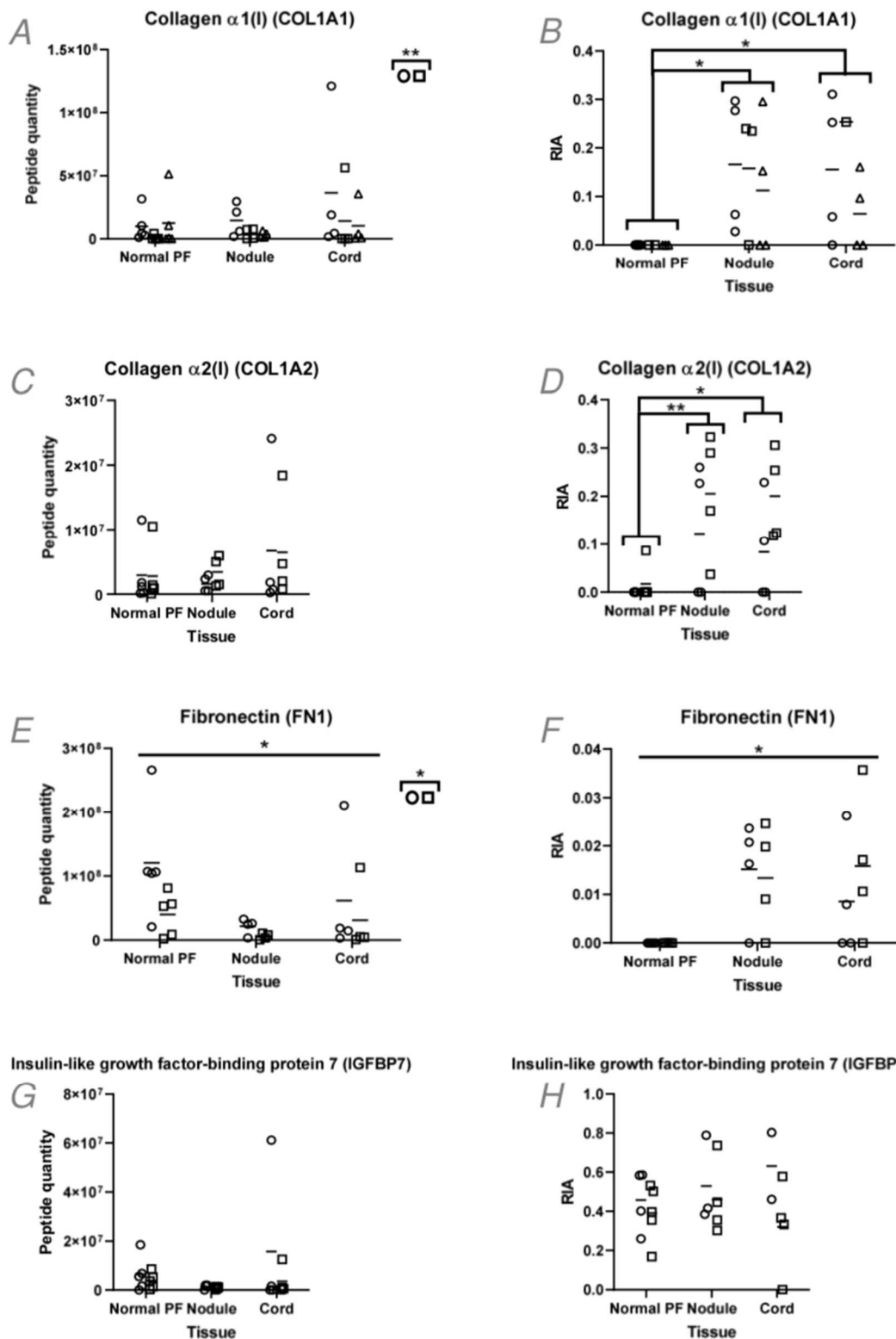
Samples were allocated for the proteomics workflow prior to final confirmation of patient age and gender information on the day of surgery. Datasets were then selected for inclusion to minimise key differences between groups and facilitate statistical analysis. Table 2 shows the age and gender distribution of the samples included in the proteomics analysis.

**Table 2: Age and gender distribution of samples analysed by proteomics.** Disease stage information (Tubiana) for Dupuytren's samples is included.

	Normal palmar fascia		Dupuytren's		
	Age	Gender	Age	Gender	Disease stage
	48	M	49	M	4
	51	F	62	F	2
	58	M	75	M	4
	68	M	76	M	2
	89	F			
<b>Mean</b>	<b>62.8</b>		<b>65.5</b>		
<b>SD</b>	<b>16.5</b>		<b>12.7</b>		

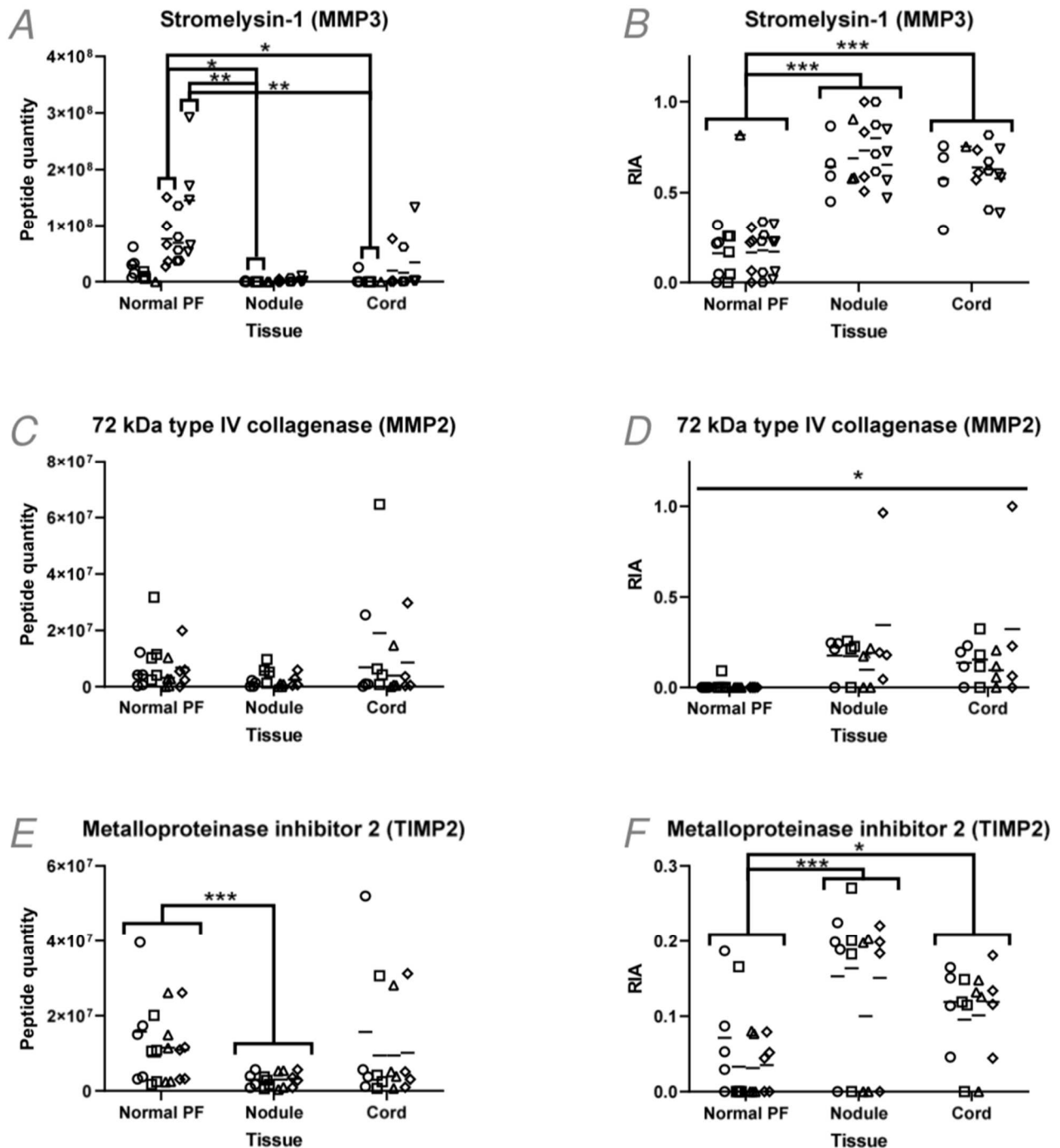
There was no significant difference in the age of samples in each group ( $p=0.796$ ). A Bayesian analysis indicated substantial evidence that there was no difference in age between the groups ( $B=0.17$ ).

To identify newly synthesized proteins in Dupuytren's nodule, cord and normal PF tissue, tissue explants were labelled with heavy lysine, and both tissue extracts and media analysed for new protein synthesis (heavy peptide content) and turnover (total peptide content) as described (Lee et al., 2019). No labelling was detected above background in tissue extracts, although labelled matrisomal proteins collagen (I) (Fig 4A-D), fibronectin (Fig 4E-F), IGFBP7 (Fig. 4G-H), MMP3 (Fig. 5A-B), MMP2 (Fig. 5C-D) and TIMP2 (Fig. 5E-F) were detected in media. Fibronectin and IGFBP7 are ECM Glycoproteins, whereas MMP3, MMP2 and TIMP2 are ECM Regulators. Of these, labelled collagen (I), MMP3 and TIMP2 were significantly higher in media from either Dupuytren's nodule or cord, than from normal PF. Fibronectin and MMP2 showed unspecified differences between sample types. Peptide quantity was not significantly reduced in normal PF media, (although was notably lower in Dupuytren's nodule or cord for MMP3 and TIMP2,) indicating that results were not skewed by explant size. Notably the relative isotope abundance for fibronectin was particularly low (<5%) and IGFBP7 was actively synthesized similarly by normal PF, Dupuytren's nodule and cord.



383  
 384 **Figure 4: Labeled core matrisomal proteins in media of normal palmar fascia (PF) and Dupuytren's tissue**  
 385 **explants.** ECM proteins labelled with  $^{13}\text{C}$  lysine were identified using MASCOT and extracted ion  
 386 chromatograms were analysed using Xcalibur. Heavy (H) and light (L) peaks were identified for each  
 387 labelled peptide and the area under the peak recorded. Total peptide quantity (H+L) normalised to  
 388 equivalent tissue weight analysed (A, C, E, G) and relative isotope abundance (RIA) (H/(L+H)) (B, D, F, H) are  
 389 shown. A&B: collagen  $\alpha 1(I)$ , C&D: collagen  $\alpha 2(I)$ , E&F: fibronectin, G&H: insulin-like growth factor-binding  
 390 protein. Different symbols represent different peptides and the bar represents the mean. \*  $p < 0.05$ , \*\*  
 391  $p < 0.01$  and \*\*\*  $p < 0.001$ .

392



393

394

395 **Figure 5: Labelled ECM Regulators in media of normal palmar fascia (PF) and Dupuytren's tissue explants.**

396 Enzymes and protein inhibitors labelled with  $^{13}\text{C}$  lysine were identified using MASCOT and extracted ion

397 chromatograms were analysed using Xcalibur. Heavy (H) and light (L) peaks were identified for each

398 labelled peptide and the area under the peak recorded. Total peptide quantity (H+L) normalised to

399 equivalent tissue weight analysed (A, C, E) and relative isotope abundance (RIA) (H/(L+H)) (B, D, F,) are

400 shown. A&B: matrix metalloproteinase 3, C&D: matrix metalloproteinase 2, E&F: tissue inhibitor of

401 metalloproteinase 2. Different symbols represent different peptides and the bar represents the mean. \*

402  $p < 0.05$ , \*\*  $p < 0.01$  and \*\*\*  $p < 0.001$ .

403

404

## 405 **TGF $\beta$ is implicated in the matrisomal profile of Dupuytren's tissue**

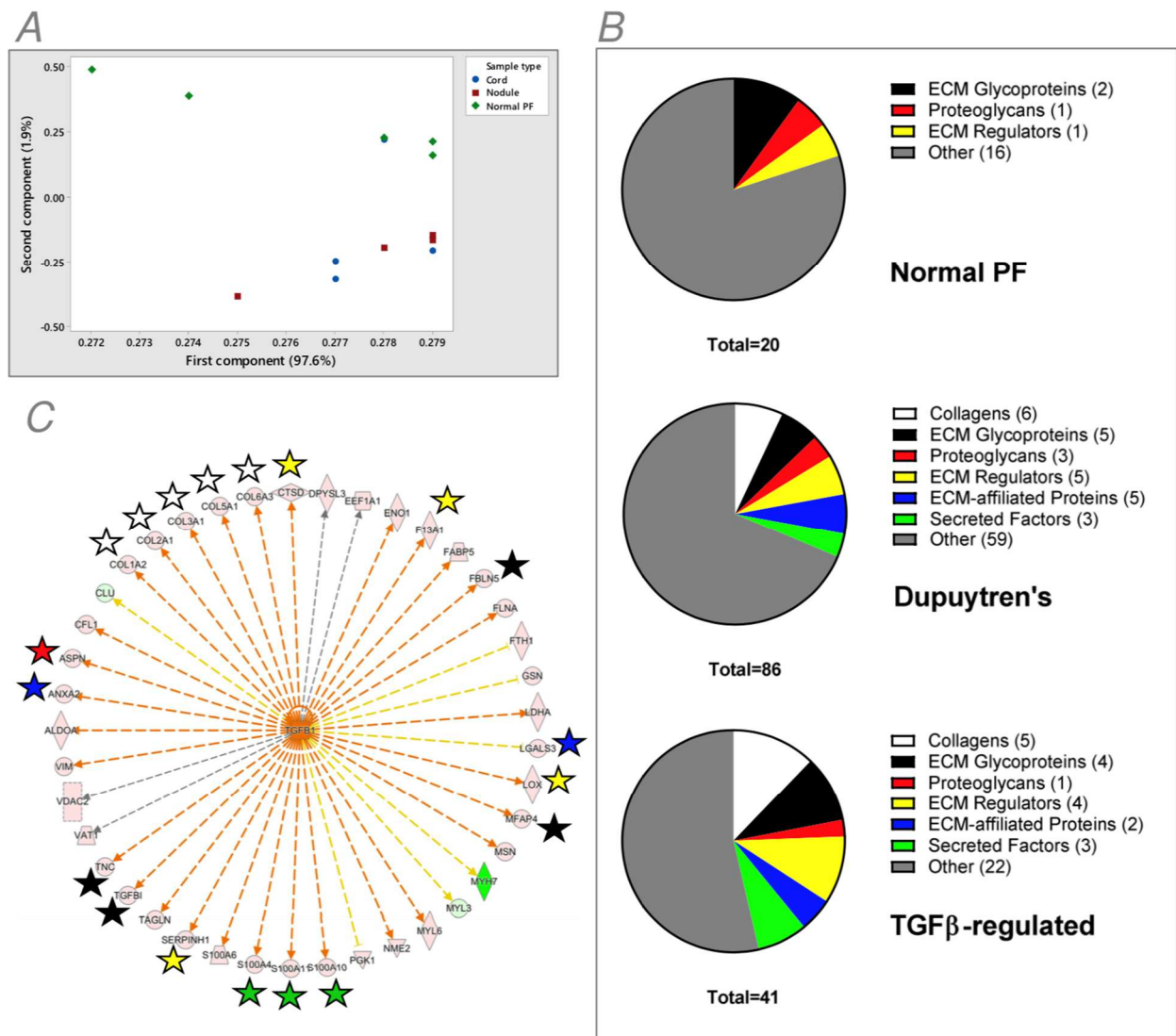
406 Label-free analysis of media and principal component analysis indicated that normal PF grouped separately  
407 from Dupuytren's media, but that nodule and cord did not cluster into discrete groups (Supplementary Fig.  
408 S1A). Matrisomal proteins comprised 31% of those proteins enriched in Dupuytren's media and TGF $\beta$  was  
409 identified as the top potential upstream regulator using Ingenuity Pathway Analysis (IPA). Of those proteins  
410 predicted to be regulated by TGF $\beta$ , 46% were matrisomal proteins (Supplementary Fig. S1B) and primarily  
411 ECM glycoproteins (Supplementary Fig. S1C). STRING protein-protein network analysis highlighted the few  
412 proteins enriched in normal PF media, including notably MMP3 (Supplementary Fig. S2A) and the well-  
413 connected cluster of matrisomal proteins enriched in Dupuytren's media (Supplementary Fig. S2B).

414 Our previous proteomic analysis of tendon and ligament tissue included a chondroitinase ABC  
415 treatment step to remove highly negatively charged glycosaminoglycans (Kharaz et al., 2016), as did earlier  
416 studies (Peffer et al., 2014; Wilson et al., 2010) and the work on which we based our guanidine/rapigest  
417 extraction methodology (Ashraf Kharaz et al., 2017). Removal of large negatively charged  
418 glycosaminoglycans could improve proteoglycan identification by improving protein digestion and peptide  
419 fractionation, but chondroitinase digestion also generates a supernatant to which some proteins could be  
420 lost. During tissue preparation in the present study the chondroitinase ABC treatment step was either  
421 omitted, or included and the chondroitinase supernatant reserved, and protein abundance compared  
422 between untreated, treated and supernatant. Heatmaps indicated some loss of proteins into the  
423 chondroitinase ABC supernatant, with increased abundance of several proteins in the supernatant of  
424 normal PF and Dupuytren's cord samples (Supplementary Fig. S3). Whilst arguably chondroitinase ABC  
425 treatment increased the detection of some proteins in Dupuytren's nodule and cord, it generally decreased  
426 detection in normal PF, and approximately equal numbers of proteins showed decreased versus increased  
427 abundance with chondroitinase treatment in Dupuytren's cord. For normal PF and cord there was evidence  
428 of some loss of proteins to the chondroitinase supernatant. Analysis was therefore performed on samples  
429 without the chondroitinase treatment step.

430 Label-free and PCA analysis of tissue processed without chondroitinase treatment again indicated  
431 that nodule and cord samples could not be distinguished on the basis of protein abundance (Fig. 6A). In the  
432 PCA one cord sample overlapped with the normal PF group. There was no overt difference in the  
433 appearance of the PCA plot for untreated and chondroitinase-treated samples (not shown). Matrisomal  
434 proteins again comprised 31% of those proteins enriched in Dupuytren's tissue and TGF $\beta$  was identified as  
435 the top potential upstream regulator using IPA. Of those proteins more abundant in Dupuytren's tissue and  
436 predicted to be regulated by TGF $\beta$ , 46% were matrisomal proteins (Fig. 6B) and were a mixture of  
437 collagens, ECM glycoproteins, ECM regulators and other matrisomal categories (Fig. 6C).

438

439



440

441

442 **Figure 6. Label-free proteomics analysis of normal palmar fascia (PF) and Dupuytren's explant tissue. A:**

443 Principal component analysis score plot grouped by tissue type. B: Enriched proteins in normal PF tissue,

444 Dupuytren's tissue and those in Dupuytren's tissue predicted to be regulated by TGFβ, subdivided based on

445 matrisomal classification. C: Ingenuity Pathway Analysis (IPA) diagram highlighting matrisomal proteins

446 within those predicted to be regulated by TGFβ. Red; increased abundance, green; decreased abundance,

447 orange; predicted to lead to activation, blue; predicted to lead to inhibition, yellow; findings inconsistent

448 with state of downstream molecule, grey; effect not predicted. Matrisomal proteins are indicated with a

449 star (collagens; white, ECM Glycoproteins; black, ECM-affiliated Proteins; blue, Proteoglycans; red, ECM

450 Regulators; yellow, Secreted Factors; green)

451

452 STRING protein-protein network analysis highlighted the few proteins enriched in normal PF tissue,

453 grouped into three small clusters (Fig. 7A), and the well-connected cluster of matrisomal proteins more

454 abundant in Dupuytren's tissue (Fig. 7B). For normal PF tissue, the top reactome pathways were amyloid

455 fiber formation (FDR 0.0051), formation of the cornified envelope (FDR 0.0106), striated muscle contraction

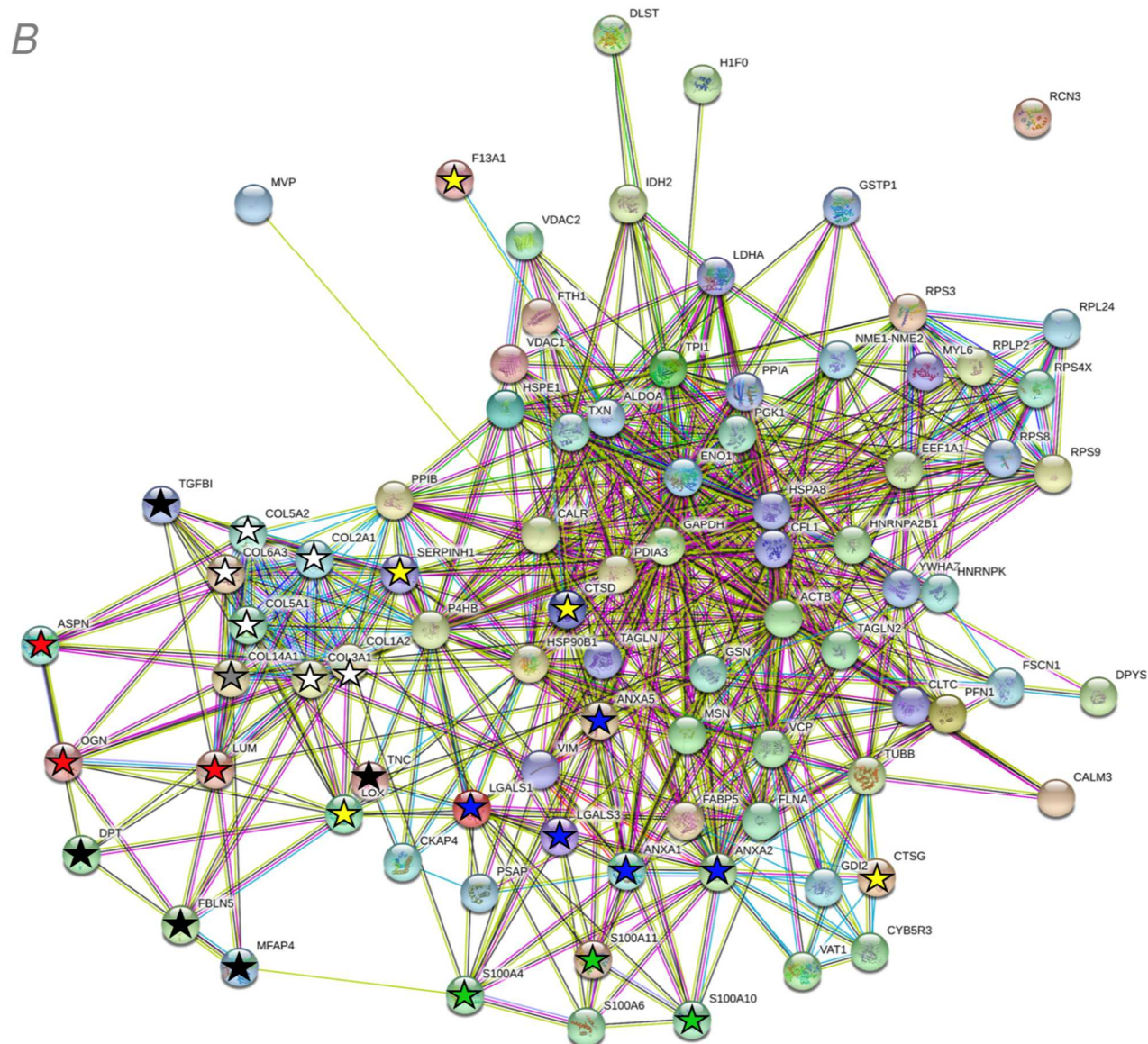
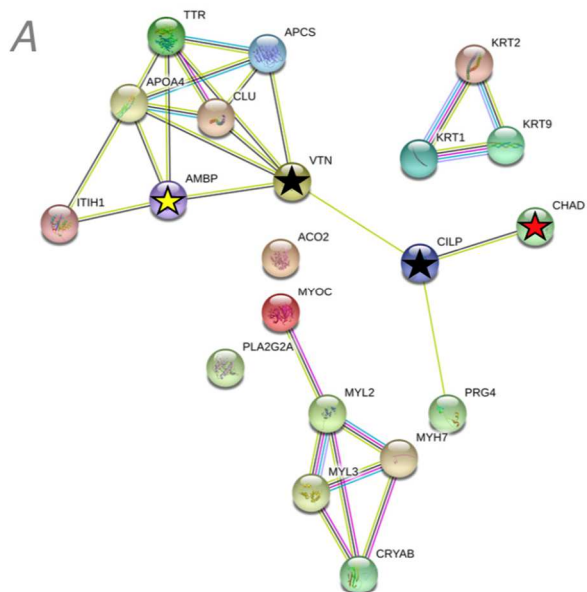
456 (FDR 0.0125), regulation of complement cascade (FDR 0.0172), and retinoid metabolism and transport (FDR

457 0.0172). For Dupuytren's tissue, the top reactome pathways were immune system (FDR 1.69e-16),

458 neutrophil degranulation (FDR 2.76e-14), extracellular matrix organization (FDR 2.25e-13), innate immune

459 system (1.46e-11), and collagen formation (4.48e-11).





462 **Figure 7. STRING interaction networks for normal palmar fascia (PF) and Dupuytren's explant tissue**  
463 **processed without chondroitinase ABC treatment.** A: Interaction network for proteins enriched in normal  
464 PF explant tissue. B: Interaction network for proteins enriched in Dupuytren's explant tissue.

465  
466

467 The large skew in protein enrichment in Dupuytren's tissue, when normalising by wet weight of tissue,  
468 indicated that proteins may be more readily extracted from Dupuytren's than normal PF. Performing the  
469 label-free analysis with a normalisation to total ion chromatogram resulted in a more even distribution  
470 between tissue types (Supplementary Fig. S4). For normal PF tissue, the top reactome pathways were  
471 integrin cell surface interactions (FDR 2.22e-09), collagen chain trimerization  
472 (FDR 5.07e-08), extracellular matrix organization (FDR 5.07e-08), assembly of collagen fibrils and other  
473 multimeric structures (FDR 1.87e-07), and collagen degradation (FDR 2.14e-07). For Dupuytren's tissue, the  
474 top reactome pathways were neutrophil degranulation (FDR 2.74e-09), immune system (FDR 3.95e-09),  
475 axon guidance (FDR 8.93e-07), innate immune system (8.93e-07), and influenza life cycle (9.84e-07).

476  
477 Given the higher protein synthesis of MMP3 by Dupuytren's nodule and cord when compared to normal PF  
478 (Fig. 5), we considered whether there were differences in peptides indicative of protein degradation  
479 between tissues. Neopeptides were identified and filtered by occurrence in at least 3 samples of normal PF  
480 explant media (Table 3), Dupuytren's explant media (Table 4), normal PF tissue (Table 5) or Dupuytren's  
481 tissue (Table 6). There were several neopeptides for CILP, TNXB, MYOC in at least 3 normal PF media and  
482 tissue samples, with MYH7 and MYOC neopeptides being present in at least 3 normal PF tissue samples but  
483 absent from Dupuytren's tissue. Two periostin neopeptides were present in at least 3 Dupuytren's nodule  
484 and cord media samples, but not in normal PF media, and three periostin neopeptides were present in at  
485 least 3 Dupuytren's nodule and cord tissue samples, but there was only one periostin neopeptide in one  
486 normal PF sample.

487  
488  
489  
490  
491  
492  
493  
494  
495  
496  
497  
498  
499  
500  
501  
502  
503  
504  
505  
506  
507

508 **Table 3: Neopeptides unique to normal palmar fascia (PF) media from  $\geq 3$  samples.** Proteins in bold have  
 509 neopeptides only in normal PF media. Brackets indicate the total number samples in which neopeptides  
 510 were identified of 5 samples total. The total number of neopeptide sequences are for that protein across all  
 511 tissue samples, hence not all unique.

<b>Protein (abbreviation)</b>	<b>Number of neopeptides unique to normal PF media (in how many samples)</b>	<b>Total number of neopeptide sequences</b>
Cartilage intermediate layer protein 1 (CILP)	7 (2 in 4; 5 in 3)	127
Myocilin (MYOC)	6 (3 in 4; 3 in 3)	128
Tenascin-X (TNXB)	6 (2 in 4; 4 in 3)	830
Neuroblast differentiation-associated protein AHNAK (AHNAK)	4 (3)	622
Procollagen C-endopeptidase enhancer 2 (PCOLCE2)	2 (1 in 4; 1 in 3)	7
<b>Alpha-crystallin B chain (CRYAB)</b>	<b>2 (4)</b>	<b>10</b>
<b>Chondroadherin (CHAD)</b>	<b>2 (1 in 5; 1 in 4)</b>	<b>10</b>
Histone H1.4 (HIST1H1E)	2 (1 in 4; 1 in 3)	15
Proteoglycan 4 (PRG4)	2 (1 in 4; 1 in 3)	20
Biglycan (BGN)	2 (1 in 4; 1 in 3)	28
Matrilin-2 (MATN2)	2 (1 in 4; 1 in 3)	31
Spectrin alpha chain, non-erythrocytic 1 (SPTAN1)	2 (3)	107
Collagen alpha-3(VI) chain (COL6A3)	2 (3)	313
Fibronectin (FN1)	2 (3)	594
<b>Ezrin (EZR)</b>	<b>1 (3)</b>	<b>3</b>
<b>Lipopolysaccharide-binding protein (LBP)</b>	<b>1 (3)</b>	<b>3</b>
<b>Ras-related protein R-Ras (RRAS)</b>	<b>1 (3)</b>	<b>3</b>
<b>Chondroitin sulfate proteoglycan 4 (CSPG4)</b>	<b>1 (3)</b>	<b>5</b>
<b>Creatine kinase M-type (CKM)</b>	<b>1 (3)</b>	<b>6</b>
PDZ and LIM domain protein 5 (PDLIM5)	1 (4)	7
<b>Ras-related protein Rap-1b (RAP1B)</b>	<b>1 (4)</b>	<b>10</b>
<b>Actin, aortic smooth muscle (ACTA2)</b>	<b>1 (3)</b>	<b>12</b>
Complement factor H-related protein 1 (CFHR1)	1(3)	17
Complement C1q subcomponent subunit B (C1QB)	1 (3)	18
Clathrin light chain B (CLTB)	1 (4)	21
Protein AMBP (AMBP)	1 (3)	22
Lactadherin (MFGE8)	1 (4)	23
Fibrillin-1 (FBN1)	1 (3)	27
Tubulin alpha-1C chain (TUBA1C)	1 (3)	32
Moesin (MSN)	1 (3)	33
Clusterin (CLU)	1 (4)	34
Extracellular superoxide dismutase [Cu-Zn] (SOD3)	1 (3)	43
Spectrin beta chain, non-erythrocytic 1 (SPTBN1)	1 (4)	47
Stromelysin-1 (MMP3)	1 (3)	51
Decorin (DCN)	1 (3)	64

<b>Procollagen C-endopeptidase enhancer 1 (PCOLCE)</b>	<b>1 (3)</b>	<b>105</b>
Fibulin-1 (FBLN1)	1 (3)	120
Plectin (PLEC)	1 (3)	202
Complement C3 (C3)	1 (3)	205
Vimentin (VIM)	1 (3)	351

512

513

514

515

516

517

**Table 4: Neopeptides unique to Dupuytren’s media from ≥3 nodule and cord samples.** Proteins in bold have neopeptides in both Dupuytren’s cord and nodule media, but not in normal palmar fascia media. Brackets indicate the total number samples in which neopeptides were identified of 4 samples total. The total number of neopeptide sequences are for that protein across all media samples, hence not all unique.

<b>Protein (abbreviation)</b>	<b>Number of neopeptides unique to Dupuytren’s media (in how many nodule, cord samples)</b>	<b>Total number of neopeptide sequences</b>
Adipocyte enhancer-binding protein 1 (AEBP1)	3 (1 in 4, 4; 2 in 3, 3)	77
<b>Periostin (POSTN)</b>	<b>2 (4, 3)</b>	<b>57</b>
Collagen alpha-1(XIV) chain (COL14A1)	2 (3, 4)	134
<b>Urotensin-2 (UTS2)</b>	<b>1 (3, 3)</b>	<b>6</b>
<b>Adenylyl cyclase-associated protein 1 (CAP1)</b>	<b>1 (3, 3)</b>	<b>8</b>
<b>Phosphatidylethanolamine-binding protein 1 (PEBP1)</b>	<b>1 (3, 4)</b>	<b>10</b>
Ribonuclease inhibitor (RNH1)	1 (3, 3)	24
Serotransferrin (TF)	1 (4, 3)	26
Olfactomedin-like protein 3 (OLFML3)	1 (4, 4)	29
Profilin-1 (PFN1)	1 (3, 3)	30
Phosphoglycerate kinase 1 (PGK1)	1 (3, 4)	31
Endoplasmic reticulum chaperone BiP (HSPA5)	1 (3, 3)	39
Hemoglobin subunit beta (HBB)	1 (3, 4)	51
Galectin-1 (LGALS1)	1 (3, 3)	69
Immunoglobulin kappa constant (IGKC)	1 (3, 3)	96
Immunoglobulin heavy constant gamma 1 (IGHG1)	1 (3, 3)	100
Actin, cytoplasmic 1 (ACTB)	1 (3, 4)	108
Collagen alpha-3(VI) chain (COL6A3)	1 (4, 4)	313
Fibronectin (FN1)	1 (4, 3)	594

518

519

520

521

522

523

524

525 **Table 5: Neopeptides unique to  $\geq 3$  normal palmar fascia (PF) tissue samples.** Proteins in bold have  
 526 neopeptides only in normal PF tissue. Brackets indicate the total number samples in which neopeptides  
 527 were identified of 4 samples total. The total number of neopeptide sequences are for that protein across all  
 528 tissue samples, hence not all unique.

Protein (abbreviation)	Number of neopeptides unique to normal PF tissue (in how many samples)	Total number of neopeptide sequences
Cartilage intermediate layer protein 1 (CILP)	10 (6 in 4; 4 in 3)	65
Tenascin-X (TNXB)	8 (2 in 5; 1 in 4; 5 in 3)	187
<b>Myosin-7 (MYH7)</b>	<b>7 (4 in 3, 3 in 4)</b>	<b>93</b>
<b>Myocilin (MYOC)</b>	<b>6 (1 in 5; 1 in 4; 4 in 3)</b>	<b>27</b>
Keratin, type II cytoskeletal 2 epidermal (KRT2)	4 (3)	25
Keratin, type I cytoskeletal 10 (KRT10)	4 (3)	74
Fibronectin (FN1)	4 (1 in 5; 3 in 4)	166
Fibrillin-1 (FBN1)	4 (1 in 5; 1 in 4; 2 in 3)	205
Vitronectin (VTN)	3 (1 in 5; 1 in 4; 1 in 3)	19
Basement membrane-specific heparan sulfate proteoglycan core protein (HSPG2)	3 (1 in 4; 1 in 3)	64
Keratin, type II cytoskeletal 1 (KRT1)	3 (2 in 5; 1 in 3)	96
Collagen alpha-2(IV) chain (COL4A2)	2 (3)	8
Protein AMBP (AMBP)	2 (2)	18
Versican core protein (VCAN)	2 (3)	20
Keratin, type I cytoskeletal 9 (KRT9)	2 (1 in 4; 1 in 3)	57
Decorin (DCN)	2 (1 in 5; 1 in 3)	88
Thrombospondin-4 (THBS4)	2 (1 in 5; 1 in 3)	112
Collagen alpha-2(I) chain (COL1A2)	2 (1 in 5; 1 in 3)	178
Collagen alpha-1(IV) chain (COL4A1)	1 (3)	4
Phospholipase A2, membrane associated (PLA2G2A)	1 (3)	4
Alpha-crystallin B chain (CRYAB)	1 (3)	5
Fibulin-1 (FBLN1)	1 (3)	6
<b>Myosin light chain 1/3, skeletal muscle isoform (MYL1)</b>	<b>1 (4)</b>	<b>7</b>
Tubulin beta-2B chain (TUBB2B)	1 (3)	8
<b>Histone H2B type 3-B (HIST3H2BB)</b>	<b>1 (5)</b>	<b>9</b>
Lactadherin (MFGE8)	1 (3)	13
EMILIN-1 (EMILIN1)	1 (4)	15
Target of Nesh-SH3 (ABI3BP)	1 (3)	20
Clusterin (CLU)	1 (5)	25
ATP synthase subunit alpha, mitochondrial (ATP5F1A)	1 (4)	31
Fibromodulin (FMOD)	1 (4)	59
Serum albumin (ALB)	1 (4)	60
Collagen alpha-2(VI) chain (COL6A2)	1 (3)	130
Cartilage oligomeric matrix protein (COMP)	1 (4)	145
Collagen alpha-1(VI) chain (COL6A1)	1 (4)	149
Collagen alpha-1(I) chain (COL1A1)	1 (3)	188

Collagen alpha-1(XII) chain (COL12A1)	1 (4)	326
Collagen alpha-3(VI) chain (COL6A3)	1 (3)	607

529

530

531

532

533

534

**Table 6: Neopeptides unique to  $\geq 3$  Dupuytren's nodule and cord samples tissue samples.** Brackets indicate the total number samples in which neopeptides were identified of 4 samples total. The total number of neopeptide sequences are for that protein across all tissue samples, hence not all unique. \* Only one POSTN neopeptide was identified in one normal palmar fascia tissue sample.

Protein (abbreviation)	Number of neopeptides unique to Dupuytren's tissue (in how many nodule, cord samples)	Total number of neopeptides for the protein
Periostin (POSTN)	3 (3, 4)	80*
Collagen alpha-1(XIV) chain (COL14A1)	2 (1 in 4, 3; 1 in 3, 3)	126
Annexin A5 (ANXA5)	1 (3)	42
Collagen alpha-1(I) chain (COL1A1)	1 (4, 3)	188
Collagen alpha-3(VI) chain (COL6A3)	1 (3, 4)	607

535

536

537

538

## Discussion

539

540

541

542

543

544

545

546

In this study, we showed increased COL1A1 and COL1A2 mRNA as well as an increased COL1A1:COL1A2 mRNA ratio in Dupuytren's tissue as compared to normal PF (Fig. 1 A-C). The results presented are in accordance with previous studies which showed increased COL1A1 mRNA in Dupuytren's tissue compared to unaffected transverse ligament of the palmar aponeurosis (Ten Dam et al., 2016) and increased COL1A1 but not COL1A2 mRNA in Dupuytren's tissue, as compared to shoulder capsule (Kilian et al., 2007). In the present study, we did not distinguish between nodule and cord for RNA analysis, although a prior study found both COL1A1 and COL1A2 mRNA was higher in nodule as compared to cord, despite lower collagen (I) protein being present in nodule (van Beuge et al., 2016).

547

548

549

550

551

552

553

554

555

556

557

558

559

One previous study indicated the presence of collagen (I) homotrimer in Dupuytren's tissue with an increase from 5% in normal PF, to 9% in Dupuytren's utilising pooled samples (Ehrlich et al., 1982). Utilising metabolic labelling with  $^{14}\text{C}$  proline, we found a consistent increase in the  $\alpha 1(\text{I}):\alpha 2(\text{I})$  polypeptide chain ratio for newly synthesised collagen in Dupuytren's tissue samples, but noted a skewed distribution with some samples showing a particularly high  $\alpha 1(\text{I}):\alpha 2(\text{I})$  chain ratio (Fig. 1 EF). We hypothesised that individual variation or samples analysed at different stages of disease progression may be responsible for the relative proportion of newly synthesised collagen however, no association with demographics data or disease stage was observed (Fig. 2). It is likely that the sample size is too low to identify factors or interactions that may direct high collagen (I) homotrimer synthesis or that the granularity of the demographics data is insufficient. The mean percentage of homotrimeric collagen is higher than that reported by Ehrlich et. al, although there is a cluster of several samples apparently synthesizing collagen (I) homotrimer to a similar extent, at around 10%. Notably our study also provides a snapshot of collagen (I) homotrimer synthesis whereas Ehrlich et. al. analysed accumulated homotrimeric collagen (I).

560

561

We noted an absence of detectable collagen (I) protein synthesis in normal PF by radiolabelling (Fig. 1D), and obtained similar results for healthy canine cranial cruciate ligament and post-natal equine

562 superficial digital flexor tendon. This indicated to us that the collagen (I) synthesis detected in Dupuytren's  
563 and ruptured cruciate ligament explants is not due to an acute injury response to dissection. In ruptured  
564 canine cranial cruciate ligament (CCL), expression of COL1A1 and COL1A2 mRNA was increased (Fig. 3 A-B).  
565 A previous study in canine CCL indicated a significant increase in COL1A2 mRNA, but not of COL1A1 in  
566 ruptured ligaments (Clements et al., 2008), whilst COL1A1 mRNA was found to be increased in ruptured  
567 human anterior cruciate ligament by in situ hybridization (Fukui et al., 2001). In the present study, the  
568 COL1A1:COL1A2 ratio was significantly higher in ruptured canine CCLs but the ratio did not exceed 2 and  
569 collagen (I) homotrimer synthesis was not apparent (Fig. 3E). Gene expression of COL1A1 and COL1A2 in  
570 equine SDFT reduced dramatically after 2 years of age (Fig. 3G) and collagen (I) protein synthesis was only  
571 detected in fetal tendon (Fig. 3F), consistent with the known high level collagen (I) expression during  
572 embryonic tendon development (Robbins and Vogel, 1994). No age-related changes in the COL1A1:COL1A2  
573 mRNA ratio were observed in equine SDFT.

574 Despite a lack of collagen (I) protein synthesis, we noted labelled bands in normal PF (Fig. 3A),  
575 canine CCL (Fig. 3E), and SDFT (Fig. 3F) tissue extracts. Attempts to identify the labelled proteins using <sup>13</sup>C  
576 proline labelling, band excision and mass spectrometry, or by Western blotting to candidate collagens were  
577 unfortunately, not informative. However, given the incorporation of <sup>14</sup>C proline, we expect that these  
578 proteins are collagenous in nature or proline-rich. Metabolic labelling with <sup>13</sup>C lysine was informative as to  
579 nascent proteins in the secretome of normal PF and Dupuytren's tissue explants. Labelled peptides for  
580 collagen  $\alpha$ 1(I) and  $\alpha$ 2(I) in Dupuytren's samples confirmed collagen (I) synthesis with up to around 30% of  
581 these peptides in the secretome being labelled (Fig. 4 A-D). The proportion of labelled fibronectin peptides  
582 was much lower, at less than 4% (Fig. 4F), implying that much of the fibronectin in the secretome leached  
583 from the tissue.

584 The presence of labelled IGBP7 peptides was an unexpected finding, being synthesized by normal  
585 PF as well as by Dupuytren's tissue (Fig. 4H). IGFBP7 has not been previously identified in tendon or  
586 ligament to our knowledge, although we previously identified IGFBP6 as a cross-species tendon marker  
587 (Turlo et al., 2019). IGFBP7 binds the IGF1 receptor to block activation by IFGs (Evdokimova et al., 2012)  
588 and has been reported to act as a tumour suppressor (Akiel et al., 2017). A role for IGFBP7 in promoting  
589 osteogenic differentiation via Wnt/ $\beta$ -catenin (Zhang et al., 2018) and as a negative regulator of  
590 osteoclastogenesis has been reported (Ye et al., 2020). Hence IGFBP7 may play an unidentified role in  
591 tendon/ligament biology.

592 Labelled peptides for MMP3 were present at higher levels in Dupuytren's nodule and cord media  
593 than in normal PF media (Fig. 5A). Labelled MMP3 peptides showed the highest <sup>13</sup>C lysine label  
594 incorporation, with up to 100% of these peptides being labelled (Fig. 5B), whilst MMP3 was more abundant  
595 in normal PF media (Fig. S2A). Hence, MMP3 is actively synthesised by Dupuytren's tissue but may have  
596 leached out of the normal PF explant into the media during labelling. MMP3 gene expression was  
597 previously shown to be lower in Dupuytren's nodule than cord; and gene expression lower in both nodule  
598 and cord regions than in normal PF from carpal tunnel patients (Johnston et al., 2007). Hence post-  
599 transcriptional mechanisms or alterations during explant culture may be responsible for the presence of  
600 newly synthesized MMP3 in Dupuytren's media. To our knowledge, no study has previously implicated  
601 MMP3 in Dupuytren's disease, but a study utilising similar methodology for the secretome of cultured  
602 cancer-associated myofibroblasts identified MMP1, MMP2 and MMP3 as rapidly incorporating heavy lysine  
603 label (Hammond et al., 2018).

604 Labelled peptides for MMP2 showed unspecified differences between samples but appeared to be  
605 more abundant in nodule and cord (Fig. 5D). MMP2 was more abundant in Dupuytren's media by label-free  
606 quantification (Fig. S2B), whilst MMP2 gene expression was previously shown to be higher in cord than  
607 nodule, with both higher than control tissue (Johnston et al., 2007) and to correlate with disease

608 recurrence (Johnston et al., 2008). Increased MMP2 activation, as detected by zymography, was also  
609 previously observed in Dupuytren's as compared to palmar fascia from carpal tunnel patients (Augoff et al.,  
610 2006). MMP2 has been shown to facilitate fibroblast-mediated collagen gel contraction (Wilkinson et al.,  
611 2012) and hence may play a role in disease progression.

612 Labelled peptides for TIMP2 were present at higher levels in Dupuytren's nodule and cord than in  
613 normal PF media (Fig. 5F) and TIMP2 itself was more abundant in Dupuytren's media (Fig. S2B). Gene  
614 expression of TIMP2 was previously shown to be lower in Dupuytren's nodule than cord or control tissue  
615 (Johnston et al., 2007). Increased MMP2 and TIMP2 mRNA but a lower MMP2:TIMP2 mRNA ratio has been  
616 demonstrated in Dupuytren's tissue (Ratajczak-Wielgomas et al., 2012). Another study also showed that  
617 Dupuytren's patients had a lower serum MMP:TIMP ratio than carpal tunnel patient controls (where MMPs  
618 represented a combined measure of MMP1, MMP2 and MMP9, and TIMPs represented a combined  
619 measure of TIMP1 and TIMP2) (Ulrich et al., 2003). A lower ratio was also observed in those patients with  
620 active as compared to inactive disease. TIMP2 is an effective inhibitor of MMP2 hence new synthesis of  
621 TIMP2 may reflect compensation for increased MMP2 synthesis or activity in Dupuytren's disease or may  
622 fine-tune MMP activity.

623 Label-free quantification and pathway analysis identified TGF $\beta$  as a likely upstream regulator of a  
624 subset of proteins more abundant in Dupuytren's tissue. Several studies have demonstrated the presence  
625 of TGF $\beta$  in Dupuytren's disease with each isoform shown to be present by immunohistochemistry  
626 (Badalamente et al., 1996; Berndt et al., 1995; Bianchi et al., 2015; Ratajczak-Wielgomas et al., 2012) and  
627 each mRNA identified by RT-PCR or in-situ hybridization (Berndt et al., 1995; Krause et al., 2011; Ratajczak-  
628 Wielgomas et al., 2012; Zhang et al., 2008). Activation of the SMAD pathway indicates an active role for  
629 TGF $\beta$  in the disease process (Krause et al., 2011) hence it is highly feasible that TGF $\beta$  regulates expression  
630 of a subset of matricellular and cellular proteins in Dupuytren's disease.

631 Reactome pathways for Dupuytren's tissue after label-free quantification included those relating to  
632 extracellular matrix/collagen and the immune system. When normalization was carried out according to  
633 the total ion chromatogram, rather than wet weight of tissue, the top reactome pathways for Dupuytren's  
634 retained descriptors relating to the immune system, whereas those relating to extracellular matrix/collagen  
635 were associated with normal PF. The increased abundance of proteins related to an immune response  
636 seems consistent with a known inflammatory response in Dupuytren's disease (Mayerl et al., 2016)  
637 although a role for neutrophils has not been previously identified in Dupuytren's; indeed no neutrophil  
638 elastase positive cells were identified by immunohistochemistry in Dupuytren's nodules (Verjee et al.,  
639 2013). The altered association of extracellular matrix/collagens pathways with Dupuytren's tissue or normal  
640 PF depending on the normalization method indicates that the extracellular matrix/collagens may be more  
641 extractable from Dupuytren's tissue than normal PF, perhaps due to more recent synthesis and hence a  
642 reduced extent of protein crosslinking. Both tissues, particularly Dupuytren's cord contain fibrillar type I  
643 collagen and extracellular matrix but these terms are more associated with Dupuytren's tissue when  
644 normalizing to the wet weight of tissue. Active ECM protein synthesis and turnover in Dupuytren's disease  
645 is highlighted by the heavy isotope labelling results (Figs 4-5) and is consistent with the fibroproliferative  
646 disease process.

647 Proteins more abundant in normal PF included those involved in muscle filament sliding such as  
648 myosin light chain 2 (MYL2), myosin light chain 3 (MYL3) and myosin heavy chain 7 (MYH7). MYH7  
649 neopeptides were also uniquely identified in normal PF (Table 5). Whilst the presence of these proteins  
650 may reflect a potential contamination from surrounding tissues, other studies have also identified  
651 transcripts more usually associated with muscle as being present in rat tendon (Mueller et al., 2016) and  
652 human Achilles (Peffer et al., 2015). Pathways relating to muscle formation were previously shown to be  
653 associated with proteins more abundant in the interfascicular matrix (endotendon) of equine SDFT than in



654 the collagenous fascicles (Thorpe et al., 2016). Thorpe et. al. obtained samples from the mid-metacarpal  
655 tendon region, far from any muscle, and utilised laser capture microdissection to prepare samples; hence  
656 contamination from surrounding tissues, or a long-range interdigitation of the myotendinous junction,  
657 seems unlikely. Ligament can contain a broader interfascicular matrix than tendon (Kharaz et al., 2018)  
658 hence muscle-related proteins in normal PF may arise from the interfascicular matrix and play a  
659 physiological role therein. The presence of proteins more usually associated with cartilage, such as  
660 cartilage intermediate layer protein 1 (CILP) and chondroadherin (CHAD) in normal PF, is consistent with  
661 previous findings of ourselves and others ligament, and may reflect the fibrocartilaginous nature of  
662 ligament regionally or throughout (Kharaz et al., 2016; Little et al., 2014). Several CILP neopeptides were  
663 identified in normal PF samples likely reflecting the abundance and turnover of CILP in ligament.

664 Myocilin was also more abundant in normal PF and myocilin neopeptides were uniquely identified  
665 in normal PF tissue (Table 5). Myocilin is found in the trabecular network of the eye and mutations are  
666 common in glaucoma (Wang et al., 2019). However myocilin has been previously identified in collagenous  
667 tissue, being enriched in male as compared to female anterior cruciate ligament (Little et al., 2014) and  
668 being identified within cells of the collagenous annulus fibrosus of the intervertebral disc (Gruber et al.,  
669 2006). Interestingly myocilin has been reported to modulate Wnt signalling (Kwon et al., 2009) whilst  
670 dysregulated Wnt signalling has been associated with Dupuytren's disease (Becker et al., 2016). Insufficient  
671 myocilin in Dupuytren's tissue may therefore promote pro-fibrotic Wnt signalling. TIMP3 has been shown  
672 to interact with myocilin to regulate MMP2 activity (Joe et al., 2017) and a dearth of myocilin in  
673 Dupuytren's tissue may result in a corresponding increase in MMP2 activity.

674 None of the neopeptides had incorporated heavy label, so were likely to have originated from the  
675 tissue itself. Several tenascin X (TNXB) neopeptides were identified in normal PF media and tissue, although  
676 tenascin X itself was not more abundant in normal PF according to the label-free analysis. Tenascin-X is a  
677 trimeric protein that plays a structural role in tissues interacting with fibrillar and FACIT collagens, as well as  
678 potentially regulating TGF $\beta$  bioavailability (Valcourt et al., 2015). Label-free analysis identified tenascin-C  
679 (TNC) as more abundant in Dupuytren's tissue and media. Tenascin-C is a hexameric matricellular protein  
680 that binds fibronectin, unlike tenascin-X and is expressed in embryonic tissues, tendon and numerous  
681 disease processes including lung and kidney fibrosis (Midwood et al., 2016). Tenascin-C often displays  
682 reciprocal expression to tenascin-X (Valcourt et al., 2015). The TNXB neopeptides in normal PF could  
683 represent a particular fragmentation process occurring during explant culture in ligament alone, or reflect  
684 the normal physiology of healthy ligament.

685 There was a striking enrichment of neopeptides from periostin (POST) in Dupuytren's media and  
686 tissue. Periostin can influence collagen fibrillogenesis, has been previously identified in periosteum,  
687 ligament, tendon and skin and is an emerging biomarker for pathological conditions (Kii, 2019). A previous  
688 study found that periostin transcripts were more abundant in Dupuytren's cord than normal PF by  
689 microarray analysis, qRT-PCR and in-situ hybridization whilst periostin protein was more abundant by  
690 Western blotting and immunohistochemistry (Vi et al., 2009). A separate study showed stronger periostin  
691 staining by immunohistochemistry in Dupuytren's tissue than in palmar fascia from carpal tunnel patients,  
692 with localized staining adjacent to  $\alpha$ -SMA positive myofibroblasts and stronger staining in earlier compared  
693 to more advanced disease stages (Ratajczak-Wielgomas et al., 2012). In the present study, utilizing a  
694 mixture of stage 2 and stage 4 (Tubiana) Dupuytren's samples, we did not identify periostin as being more  
695 abundant in Dupuytren's tissue by label-free proteomics and a prior proteomics study comparing residual  
696 disease stage Dupuytren's tissue to adjacent unaffected palmar fascia similarly did not detect differential  
697 abundance of periostin (Kraljevic Pavelic et al., 2009). The neopeptides identified in the present study could  
698 have arisen from fragmentation over the course of the explant culture carried out for metabolic labelling,  
699 or from prior fragmentation within the tissue during disease progression.

700           There were numerous collagen (I) neopeptides present in normal PF and Dupuytren's tissue. None  
701 of the neopeptides corresponded to the MMP cleavage site in collagen (I), indicating that the peptides  
702 likely arose from later gelatinase activity. Only one alpha-1(I) chain neopeptide was present in at least three  
703 Dupuytren's cord and nodule samples, whilst for normal PF there was only one alpha-1(I) chain and two  
704 alpha-2(I) chain neopeptides that were present in at least three samples. New type I collagen synthesis in  
705 Dupuytren's tissue and media was confirmed by radio- and heavy-isotope labelling approaches, whilst the  
706 label-free analysis indicated that the alpha-2(I) chain (COL1A2), but not the alpha-1(I) chain (COL1A1) was  
707 more abundant in Dupuytren's tissue and media. This could reflect differences in extractability of  
708 previously synthesised heterotrimeric and homotrimeric collagen (I) molecules due to altered crosslinking  
709 (Pfeiffer et al., 2005). In this study, we used an extraction method for the insoluble pellet previously shown  
710 to increase the identification of collagenous proteins (Ashraf Kharaz et al., 2017) However, it may be that  
711 pepsinisation of the insoluble pellet (Peffer et al., 2014) to break mature crosslinks between telopeptides  
712 would have released more homotrimeric collagen (I), and hence alpha-1(I) chain (COL1A1) peptides from  
713 Dupuytren's tissue.

714           In conclusion, we have shown that Dupuytren's tissue actively synthesizes both homotrimeric and  
715 heterotrimeric type I collagen as well as MMP3 and TIMP2, supporting our hypothesis of a continual  
716 abnormal production of ECM proteins in Dupuytren's. Label-free proteomics implicated the TGF $\beta$ TGF $\beta$   
717 pathway in the profile of matrisomal proteins in Dupuytren's tissue whilst a lack of myocilin could  
718 contribute to aberrant Wnt signalling in Dupuytren's disease. The continual synthesis of collagen-1, MMPs  
719 and TIMPs together with TGF $\beta$  and Wnt pathway activation could therefore contribute to disease  
720 recurrence by promoting persistent collagen deposition and tissue remodeling.

721  
722

## 723 **Author contributions**

724 Conceptualization: EGC-L. Funding acquisition: EGC-L. Resources: GCh, DB, RP, EVC, PDC. Methodology:  
725 KAW, KJL, EGC-L. Investigation: KAW, KJL, EB, DS, AC, JAG. Data curation: KAW, KJL, EB, DS, EGC-L. Project  
726 administration: RP, EVC, PDC, EGC-L. Supervision: EVC, PDC, EGC-L. Formal Analysis: KAW, KJL, EB, EGC-L.  
727 Visualization: KAW, KJL, EB, EGC-L. Writing – original draft: EGC-L. Writing – review & editing: KAW, KJL, EB,  
728 DS, JAG, GCh, DB, RP, EVC, PDC, EGC-L.

729  
730

## 731 **Acknowledgements**

732 The assistance of the surgical teams and research nurses at the Royal Liverpool and Broadgreen University  
733 Hospitals NHS Trust and the Warrington and Halton Hospitals NHS Foundation Trust, as well as the  
734 contribution of the patients donating samples for the study is gratefully acknowledged. The authors would  
735 like to thank the staff at the Philip Leverhulme Equine Hospital and the Small Animal Teaching Hospital, as  
736 well as the owners that donated tissue for use in research. The authors are also grateful for the assistance  
737 of Professor Rob Beynon for advice on study design and data analysis; Gabriella Cooper for processing  
738 samples and proofreading; and Professor Mandy Peffer in providing advice, a protocol and template for  
739 the neopeptide analysis. The invaluable assistance of Mr Adrian Chojnowski at the Norfolk and Norwich  
740 University Hospitals NHS Foundation Trust, and Dr Graham Riley and Professor Ian Clark at the University of  
741 East Anglia in providing human surgical samples (REC 10/H0310/03) early in the study is gratefully  
742 acknowledged.

743           This study was funded by the UK Medical Research Council (MRC) (MR/J002909) and the Dowager  
744 Countess Eleanor Peel Trust (DCEPT) (#148). KJL was supported by the Marjorie Forrest Bequest and by the  
745 Institute of Ageing and Chronic Disease at the University of Liverpool and now by MRC (MR/R00319X/1).

746 ELB is supported by Versus Arthritis (21809). JAG was supported by The Medical Research Council Versus  
747 Arthritis Centre for Integrated Research into Musculoskeletal Ageing (CIMA).

748  
749

## 750 References

- 751 Akiel, M., C. Guo, X. Li, D. Rajasekaran, R.G. Mendoza, C.L. Robertson, N. Jariwala, F. Yuan, M.A. Subler, J.  
752 Windle, D.K. Garcia, Z. Lai, H.H. Chen, Y. Chen, S. Giashuddin, P.B. Fisher, X.Y. Wang, and D. Sarkar.  
753 2017. IGFBP7 Deletion Promotes Hepatocellular Carcinoma. *Cancer Res.* 77:4014-4025.
- 754 Ali, O.J., E.J. Comerford, P.D. Clegg, and E.G. Canty-Laird. 2018. Variations during ageing in the three-  
755 dimensional anatomical arrangement of fascicles within the equine superficial digital flexor tendon.  
756 *Eur Cell Mater.* 35:87-102.
- 757 Angi, M., H. Kalirai, S. Prendergast, D. Simpson, D.E. Hammond, M.C. Madigan, R.J. Beynon, and S.E.  
758 Coupland. 2016. In-depth proteomic profiling of the uveal melanoma secretome. *Oncotarget.*  
759 7:49623-49635.
- 760 Ashraf Kharaz, Y., D. Zamboulis, K. Sanders, E. Comerford, P. Clegg, and M. Peffers. 2017. Comparison  
761 between chaotropic and detergent-based sample preparation workflow in tendon for mass  
762 spectrometry analysis. *Proteomics.* 17.
- 763 Augoff, K., K. Ratajczak, J. Gosk, R. Tabola, and R. Rutowski. 2006. Gelatinase A activity in Dupuytren's  
764 disease. *J Hand Surg Am.* 31:1635-1639.
- 765 Badalamente, M.A., S.P. Sampson, L.C. Hurst, A. Dowd, and K. Miyasaka. 1996. The role of transforming  
766 growth factor beta in Dupuytren's disease. *J Hand Surg Am.* 21:210-215.
- 767 Becker, K., S. Siegert, M.R. Toliat, J. Du, R. Casper, G.H. Dolmans, P.M. Werker, S. Tinschert, A. Franke, C.  
768 Gieger, K. Strauch, M. Nothnagel, P. Nurnberg, H.C. Hennies, and G. German Dupuytren Study.  
769 2016. Meta-Analysis of Genome-Wide Association Studies and Network Analysis-Based Integration  
770 with Gene Expression Data Identify New Suggestive Loci and Unravel a Wnt-Centric Network  
771 Associated with Dupuytren's Disease. *PLoS One.* 11:e0158101.
- 772 Berndt, A., H. Kosmehl, U. Mandel, U. Gabler, X. Luo, D. Celeda, L. Zardi, and D. Katenkamp. 1995. TGF beta  
773 and bFGF synthesis and localization in Dupuytren's disease (nodular palmar fibromatosis) relative  
774 to cellular activity, myofibroblast phenotype and oncofetal variants of fibronectin. *Histochem J.*  
775 27:1014-1020.
- 776 Bianchi, E., S. Taurone, L. Bardella, A. Signore, E. Pompili, V. Sessa, C. Chiappetta, L. Fumagalli, C. Di Gioia,  
777 F.S. Pastore, S. Scarpa, and M. Artico. 2015. Involvement of pro-inflammatory cytokines and growth  
778 factors in the pathogenesis of Dupuytren's contracture: a novel target for a possible future  
779 therapeutic strategy? *Clin Sci (Lond).* 129:711-720.
- 780 Brickley-Parsons, D., M.J. Glimcher, R.J. Smith, R. Albin, and J.P. Adams. 1981. Biochemical changes in the  
781 collagen of the palmar fascia in patients with Dupuytren's disease. *J Bone Joint Surg Am.* 63:787-  
782 797.
- 783 Clements, D.N., S.D. Carter, J.F. Innes, W.E. Ollier, and P.J. Day. 2008. Gene expression profiling of normal  
784 and ruptured canine anterior cruciate ligaments. *Osteoarthritis Cartilage.* 16:195-203.
- 785 Craxford, S., and P.G. Russell. 2016. Dupuytren's disease. *Surgery (Oxford).* 34:139-143.
- 786 Dibenedetti, D.B., D. Nguyen, L. Zografos, R. Ziemiecki, and X. Zhou. 2011. Prevalence, incidence, and  
787 treatments of Dupuytren's disease in the United States: results from a population-based study.  
788 *Hand.* 6:149-158.
- 789 Dienes, Z. 2014. Using Bayes to get the most out of non-significant results. *Frontiers in Psychology.* 5.
- 790 Ehrlich, H.P., H. Brown, and B.S. White. 1982. Evidence for type V and I trimer collagens in Dupuytren's  
791 Contracture palmar fascia. *Biochem Med.* 28:273-284.
- 792 Evdokimova, V., C.E. Tognon, T. Benatar, W. Yang, K. Krutikov, M. Pollak, P.H. Sorensen, and A. Seth. 2012.  
793 IGFBP7 binds to the IGF-1 receptor and blocks its activation by insulin-like growth factors. *Sci*  
794 *Signal.* 5:ra92.
- 795 Forrester, H.B., P. Temple-Smith, S. Ham, D. de Kretser, G. Southwick, and C.N. Sprung. 2013. Genome-wide  
796 analysis using exon arrays demonstrates an important role for expression of extra-cellular matrix,  
797 fibrotic control and tissue remodelling genes in Dupuytren's disease. *PLoS One.* 8:e59056.

- 798 Fukui, N., Y. Katsuragawa, A. Kawakami, H. Sakai, H. Oda, and K. Nakamura. 2001. Metabolic activity in  
799 disrupted human anterior cruciate ligament. Evaluation of procollagen mRNA expression in 29  
800 patients. *Joint Bone Spine*. 68:318-326.
- 801 Grazina, R., S. Teixeira, R. Ramos, H. Sousa, A. Ferreira, and R. Lemos. 2019. Dupuytren's disease: where do  
802 we stand? *EFORT Open Rev*. 4:63-69.
- 803 Gruber, H.E., J.A. Ingram, and E.N. Hanley, Jr. 2006. Cellular immunohistochemical localization of the  
804 matricellular protein myocilin in the intervertebral disc. *Biotech Histochem*. 81:119-124.
- 805 Hammond, D.E., J.D. Kumar, L. Raymond, D.M. Simpson, R.J. Beynon, G.J. Dockray, and A. Varro. 2018.  
806 Stable Isotope Dynamic Labeling of Secretomes (SIDLS) Identifies Authentic Secretory Proteins  
807 Released by Cancer and Stromal Cells. *Molecular & cellular proteomics : MCP*. 17:1837-1849.
- 808 Hindocha, S., D.A. McGruther, and A. Bayat. 2009. Epidemiological evaluation of Dupuytren's disease  
809 incidence and prevalence rates in relation to etiology. *Hand*. 4:256-269.
- 810 Hindocha, S., J.K. Stanley, J.S. Watson, and A. Bayat. 2008. Revised Tubiana's staging system for assessment  
811 of disease severity in Dupuytren's disease-preliminary clinical findings. *Hand*. 3:80-86.
- 812 Joe, M.K., R.L. Lieberman, N. Nakaya, and S.I. Tomarev. 2017. Myocilin Regulates Metalloprotease 2 Activity  
813 Through Interaction With TIMP3. *Invest Ophthalmol Vis Sci*. 58:5308-5318.
- 814 Johnston, P., A.J. Chojnowski, R.K. Davidson, G.P. Riley, S.T. Donell, and I.M. Clark. 2007. A Complete  
815 Expression Profile of Matrix-Degrading Metalloproteinases in Dupuytren's Disease. *The Journal of*  
816 *Hand Surgery*. 32:343-351.
- 817 Johnston, P., D. Larson, I.M. Clark, and A.J. Chojnowski. 2008. Metalloproteinase gene expression correlates  
818 with clinical outcome in Dupuytren's disease. *J Hand Surg Am*. 33:1160-1167.
- 819 Jung, J., G.W. Kim, B. Lee, J.W.J. Joo, and W. Jang. 2019. Integrative genomic and transcriptomic analysis of  
820 genetic markers in Dupuytren's disease. *BMC Med Genomics*. 12:98.
- 821 Kharaz, Y.A., E.G. Canty-Laird, S.R. Tew, and E.J. Comerford. 2018. Variations in internal structure,  
822 composition and protein distribution between intra- and extra-articular knee ligaments and  
823 tendons. *J Anat*. 232:943-955.
- 824 Kharaz, Y.A., S.R. Tew, M. Peffers, E.G. Canty-Laird, and E. Comerford. 2016. Proteomic differences between  
825 native and tissue-engineered tendon and ligament. *Proteomics*. 16:1547-1556.
- 826 Kii, I. 2019. Practical Application of Periostin as a Biomarker for Pathological Conditions. *Adv Exp Med Biol*.  
827 1132:195-204.
- 828 Kilian, O., U. Pfeil, S. Wenisch, C. Heiss, R. Kraus, and R. Schnettler. 2007. Enhanced alpha 1(I) mRNA  
829 expression in frozen shoulder and dupuytren tissue. *Eur J Med Res*. 12:585-590.
- 830 Kraljevic Pavelic, S., M. Sedic, K. Hock, S. Vucinic, D. Jurisic, P. Gehrig, M. Scott, R. Schlapbach, T. Cacev, S.  
831 Kapitanovic, and K. Pavelic. 2009. An integrated proteomics approach for studying the molecular  
832 pathogenesis of Dupuytren's disease. *The Journal of pathology*. 217:524-533.
- 833 Krause, C., P. Kloen, and P. Ten Dijke. 2011. Elevated transforming growth factor beta and mitogen-  
834 activated protein kinase pathways mediate fibrotic traits of Dupuytren's disease fibroblasts.  
835 *Fibrogenesis Tissue Repair*. 4:14.
- 836 Krefter, C., M. Marks, S. Hensler, D.B. Herren, and M. Calcagni. 2017. Complications after treating  
837 Dupuytren's disease. A systematic literature review. *Hand Surg Rehabil*. 36:322-329.
- 838 Kwon, H.S., H.S. Lee, Y. Ji, J.S. Rubin, and S.I. Tomarev. 2009. Myocilin is a modulator of Wnt signaling. *Mol*  
839 *Cell Biol*. 29:2139-2154.
- 840 Lam, W.L., J.M. Rawlins, R.O. Karoo, I. Naylor, and D.T. Sharpe. 2010. Re-visiting Luck's classification: a  
841 histological analysis of Dupuytren's disease. *J Hand Surg Eur Vol*. 35:312-317.
- 842 Layton, T., and J. Nanchahal. 2019. Recent advances in the understanding of Dupuytren's disease.  
843 *F1000Res*. 8.
- 844 Lee, K.J., P.D. Clegg, E.J. Comerford, and E.G. Canty-Laird. 2018. A comparison of the stem cell  
845 characteristics of murine tenocytes and tendon-derived stem cells. *BMC Musculoskelet Disord*.  
846 19:116.
- 847 Lee, K.J., E.J. Comerford, D.M. Simpson, P.D. Clegg, and E.G. Canty-Laird. 2019. Identification and  
848 Characterization of Canine Ligament Progenitor Cells and Their Extracellular Matrix Niche. *J*  
849 *Proteome Res*. 18:1328-1339.

- 850 Little, D., J.W. Thompson, L.G. Dubois, D.S. Ruch, M.A. Moseley, and F. Guilak. 2014. Proteomic differences  
851 between male and female anterior cruciate ligament and patellar tendon. *PLoS One*. 9:e96526.
- 852 Luck, J.V. 1959. Dupuytren's contracture; a new concept of the pathogenesis correlated with surgical  
853 management. *J Bone Joint Surg Am*. 41-A:635-664.
- 854 Makareeva, E., S. Han, J.C. Vera, D.L. Sackett, K. Holmbeck, C.L. Phillips, R. Visse, H. Nagase, and S. Leikin.  
855 2010. Carcinomas Contain a Matrix Metalloproteinase-Resistant Isoform of Type I Collagen  
856 Exerting Selective Support to Invasion. *Cancer Res*. 70:4366-4374.
- 857 Mayerl, C., B. Del Frari, W. Parson, G. Boeck, H. Piza-Katzer, G. Wick, and D. Wolfram. 2016.  
858 Characterisation of the inflammatory response in Dupuytren's disease. *J Plast Surg Hand Surg*.  
859 50:171-179.
- 860 Midwood, K.S., M. Chiquet, R.P. Tucker, and G. Orend. 2016. Tenascin-C at a glance. *J Cell Sci*. 129:4321-  
861 4327.
- 862 Mueller, A.J., S.R. Tew, O. Vasieva, P.D. Clegg, and E.G. Canty-Laird. 2016. A systems biology approach to  
863 defining regulatory mechanisms for cartilage and tendon cell phenotypes. *Scientific reports*.  
864 6:33956.
- 865 Ng, M., D. Thakkar, L. Southam, P. Werker, R. Ophoff, K. Becker, M. Nothnagel, A. Franke, P. Nurnberg, A.I.  
866 Espirito-Santo, D. Izadi, H.C. Hennies, J. Nanchahal, E. Zeggini, and D. Furniss. 2017. A Genome-wide  
867 Association Study of Dupuytren Disease Reveals 17 Additional Variants Implicated in Fibrosis. *Am J*  
868 *Hum Genet*. 101:417-427.
- 869 Peffers, M.J., Y. Fang, K. Cheung, T.K. Wei, P.D. Clegg, and H.L. Birch. 2015. Transcriptome analysis of ageing  
870 in uninjured human Achilles tendon. *Arthritis Res Ther*. 17:33.
- 871 Peffers, M.J., C.T. Thorpe, J.A. Collins, R. Eong, T.K. Wei, H.R. Screen, and P.D. Clegg. 2014. Proteomic  
872 analysis reveals age-related changes in tendon matrix composition, with age- and injury-specific  
873 matrix fragmentation. *Journal of Biological Chemistry*. 289:25867-25878.
- 874 Pfeiffer, B.J., C.L. Franklin, F.H. Hsieh, R.A. Bank, and C.L. Phillips. 2005. Alpha 2(I) collagen deficient oim  
875 mice have altered biomechanical integrity, collagen content, and collagen crosslinking of their  
876 thoracic aorta. *Matrix Biol*. 24:451-458.
- 877 Ratajczak-Wielgomas, K., J. Gosk, J. Rabczynski, K. Augoff, M. Podhorska-Okolow, A. Gamian, and R.  
878 Rutowski. 2012. Expression of MMP-2, TIMP-2, TGF-beta1, and decorin in Dupuytren's contracture.  
879 *Connect Tissue Res*. 53:469-477.
- 880 Riester, S.M., D. Arsoy, E.T. Camilleri, A. Dudakovic, C.R. Paradise, J.M. Evans, J. Torres-Mora, M. Rizzo, P.  
881 Kloen, M.K. Julio, A.J. van Wijnen, and S. Kakar. 2015. RNA sequencing reveals a depletion of  
882 collagen targeting microRNAs in Dupuytren's disease. *BMC Med Genomics*. 8:59.
- 883 Robbins, J.R., and K.G. Vogel. 1994. Regional expression of mRNA for proteoglycans and collagen in tendon.  
884 *Eur J Cell Biol*. 64:264-270.
- 885 Shih, B., S. Watson, and A. Bayat. 2012. Whole genome and global expression profiling of Dupuytren's  
886 disease: systematic review of current findings and future perspectives. *Ann Rheum Dis*. 71:1440-  
887 1447.
- 888 Soreide, E., M.H. Murad, J.M. Denbeigh, E.A. Lewallen, A. Dudakovic, L. Nordsletten, A.J. van Wijnen, and S.  
889 Kakar. 2018. Treatment of Dupuytren's contracture: a systematic review. *Bone Joint J*. 100-B:1138-  
890 1145.
- 891 Sykes, B., B. Puddle, M. Francis, and R. Smith. 1976. The estimation of two collagens from human dermis by  
892 interrupted gel electrophoresis. *Biochem Biophys Res Commun*. 72:1472-1480.
- 893 Szklarczyk, D., A.L. Gable, D. Lyon, A. Junge, S. Wyder, J. Huerta-Cepas, M. Simonovic, N.T. Doncheva, J.H.  
894 Morris, P. Bork, L.J. Jensen, and C.V. Mering. 2019. STRING v11: protein-protein association  
895 networks with increased coverage, supporting functional discovery in genome-wide experimental  
896 datasets. *Nucleic Acids Res*. 47:D607-D613.
- 897 Tan, K., A.H.J. Withers, S.T. Tan, and T. Itinteang. 2018. The Role of Stem Cells in Dupuytren's Disease: A  
898 Review. *Plast Reconstr Surg Glob Open*. 6:e1777.
- 899 Ten Dam, E.J., M.M. van Beuge, R.A. Bank, and P.M. Werker. 2016. Further evidence of the involvement of  
900 the Wnt signaling pathway in Dupuytren's disease. *J Cell Commun Signal*. 10:33-40.

- 901 Thorpe, C.T., M.J. Peffers, D. Simpson, E. Halliwell, H.R. Screen, and P.D. Clegg. 2016. Anatomical  
902 heterogeneity of tendon: Fascicular and interfascicular tendon compartments have distinct  
903 proteomic composition. *Scientific reports*. 6:20455.
- 904 Tomasek, J.J., and C.J. Haaksma. 1991. Fibronectin filaments and actin microfilaments are organized into a  
905 fibronexus in Dupuytren's diseased tissue. *Anat Rec*. 230:175-182.
- 906 Turlo, A.J., A.J. Mueller-Breckenridge, D.E. Zamboulis, S.R. Tew, E.G. Canty-Laird, and P.D. Clegg. 2019.  
907 Insulin-like growth factor binding protein (IGFBP6) is a cross-species tendon marker. *Eur Cell Mater*.  
908 38:123-136.
- 909 Ulrich, D., K. Hrynyschyn, and N. Pallua. 2003. Matrix metalloproteinases and tissue inhibitors of  
910 metalloproteinases in sera and tissue of patients with Dupuytren's disease. *Plast Reconstr Surg*.  
911 112:1279-1286.
- 912 Valcourt, U., L.B. Alcaraz, J.Y. Exposito, C. Lethias, and L. Bartholin. 2015. Tenascin-X: beyond the  
913 architectural function. *Cell Adh Migr*. 9:154-165.
- 914 van Beuge, M.M., E.J. Ten Dam, P.M. Werker, and R.A. Bank. 2016. Matrix and cell phenotype differences in  
915 Dupuytren's disease. *Fibrogenesis Tissue Repair*. 9:9.
- 916 Verjee, L.S., K. Midwood, D. Davidson, D. Essex, A. Sandison, and J. Nanchahal. 2009. Myofibroblast  
917 distribution in Dupuytren's cords: correlation with digital contracture. *J Hand Surg Am*. 34:1785-  
918 1794.
- 919 Verjee, L.S., J.S. Verhoekx, J.K. Chan, T. Krausgruber, V. Nicolaidou, D. Izadi, D. Davidson, M. Feldmann, K.S.  
920 Midwood, and J. Nanchahal. 2013. Unraveling the signaling pathways promoting fibrosis in  
921 Dupuytren's disease reveals TNF as a therapeutic target. *Proc Natl Acad Sci U S A*. 110:E928-937.
- 922 Vi, L., L. Feng, R.D. Zhu, Y. Wu, L. Satish, B.S. Gan, and D.B. O'Gorman. 2009. Periostin differentially induces  
923 proliferation, contraction and apoptosis of primary Dupuytren's disease and adjacent palmar fascia  
924 cells. *Exp Cell Res*. 315:3574-3586.
- 925 Wang, H., M. Li, Z. Zhang, H. Xue, X. Chen, and Y. Ji. 2019. Physiological function of myocilin and its role in  
926 the pathogenesis of glaucoma in the trabecular meshwork (Review). *International journal of*  
927 *molecular medicine*. 43:671-681.
- 928 Wilkinson, J.M., R.K. Davidson, T.E. Swingler, E.R. Jones, A.N. Corps, P. Johnston, G.P. Riley, A.J. Chojnowski,  
929 and I.M. Clark. 2012. MMP-14 and MMP-2 are key metalloproteases in Dupuytren's disease  
930 fibroblast-mediated contraction. *Biochimica et Biophysica Acta (BBA) - Molecular Basis of Disease*.  
931 1822:897-905.
- 932 Wilson, R., A.F. Diseberg, L. Gordon, S. Zivkovic, L. Tatarczuch, E.J. Mackie, J.J. Gorman, and J.F. Bateman.  
933 2010. Comprehensive profiling of cartilage extracellular matrix formation and maturation using  
934 sequential extraction and label-free quantitative proteomics. *Molecular & cellular proteomics :*  
935 *MCP*. 9:1296-1313.
- 936 Worrell, M. 2012. Dupuytren's disease. *Orthopedics*. 35:52-60.
- 937 Wynn, T.A. 2008. Cellular and molecular mechanisms of fibrosis. *The Journal of pathology*. 214:199-210.
- 938 Ye, C., W. Hou, M. Chen, J. Lu, E. Chen, L. Tang, K. Hang, Q. Ding, Y. Li, W. Zhang, and R. He. 2020. IGFBP7  
939 acts as a negative regulator of RANKL-induced osteoclastogenesis and oestrogen deficiency-  
940 induced bone loss. *Cell Prolif*. 53:e12752.
- 941 Zeisberg, M., and R. Kalluri. 2013. Cellular mechanisms of tissue fibrosis. 1. Common and organ-specific  
942 mechanisms associated with tissue fibrosis. *Am J Physiol Cell Physiol*. 304:C216-225.
- 943 Zhang, A.Y., K.D. Fong, H. Pham, R.P. Nacamuli, M.T. Longaker, and J. Chang. 2008. Gene expression analysis  
944 of Dupuytren's disease: the role of TGF-beta2. *J Hand Surg Eur Vol*. 33:783-790.
- 945 Zhang, W., E. Chen, M. Chen, C. Ye, Y. Qi, Q. Ding, H. Li, D. Xue, X. Gao, and Z. Pan. 2018. IGFBP7 regulates  
946 the osteogenic differentiation of bone marrow-derived mesenchymal stem cells via Wnt/beta-  
947 catenin signaling pathway. *FASEB J*. 32:2280-2291.
- 948  
949  
950  
951  
952  
953

954  
955  
956  
957  
958  
959  
960  
961  
962  
963  
964  
965  
966  
967  
968  
969  
970  
971  
972  
973  
974  
975  
976  
977  
978  
979  
980  
981  
982  
983  
984  
985  
986  
987  
988  
989  
990  
991  
992  
993  
994  
995  
996  
997  
998  
999  
1000  
1001  
1002  
1003  
1004

## Supplementary Results

### Variability in metabolic labelling between Dupuytren's tissue explants

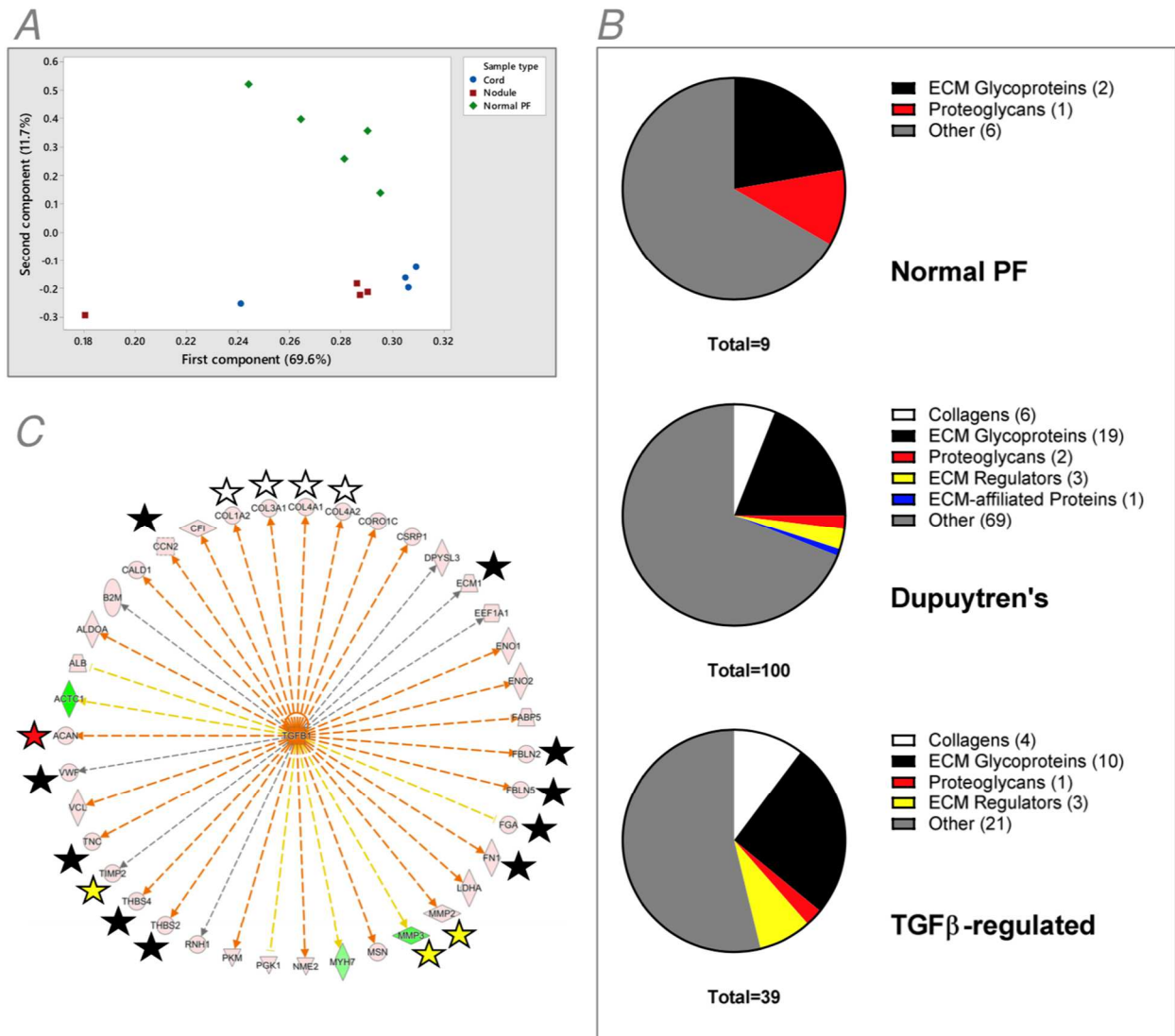
Samples derived from 4 of 31 patients were insufficiently labelled for densitometric quantification. Some patients donated samples from more than one digit. In others, cord and nodule were distinct and hence processed separately.

For 2 patients gifting samples relating to different digits the sample from only the thumb (and not the ring/little or little finger) was labelled. For one patient neither the samples donated from the little or ring finger were labelled. No labelled samples from multiple digits from the same patient were obtained.

For 2 of 5 patients, with samples for which both cord and nodule were processed, only the nodule was sufficiently labelled for quantification. For samples for which both cord and nodule were processed, the mean value for the ratio was used for analyses.

1005  
1006  
1007  
1008  
1009

## Supplementary Figures

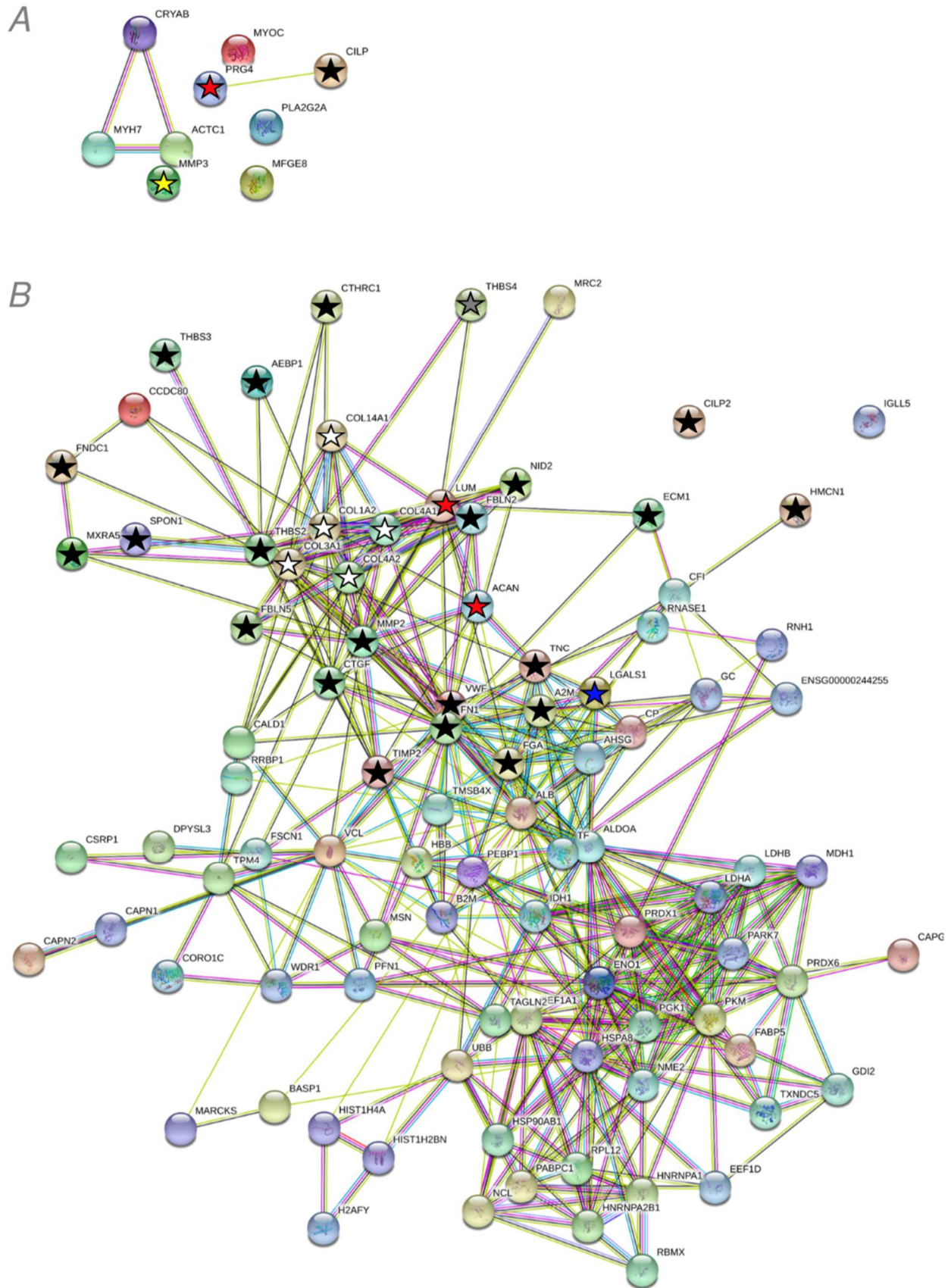


1010  
1011  
1012  
1013  
1014  
1015  
1016  
1017  
1018  
1019  
1020  
1021

**Supplementary Figure S1. Label-free proteomics analysis of normal palmar fascia (PF) and Dupuytren's explant media.** A: Principal component analysis score plot grouped by tissue type. B: Enriched proteins in normal PF media, Dupuytren's media and those in Dupuytren's media predicted to be regulated by TGF $\beta$ , subdivided based on matrisomal classification. C: Ingenuity Pathway Analysis diagram highlighting matrisomal proteins within those predicted to be regulated by TGF $\beta$ . Red; increased abundance, green; decreased abundance, orange; predicted to lead to activation, blue; predicted to lead to inhibition, yellow; findings inconsistent with state of downstream molecule, grey; effect not predicted. Matrisomal proteins are indicated with a star (collagens; white, Extracellular Matrix [ECM] Glycoproteins; black, ECM-affiliated Proteins; blue, Proteoglycans; red, ECM Regulators; yellow, Secreted Factors; green).



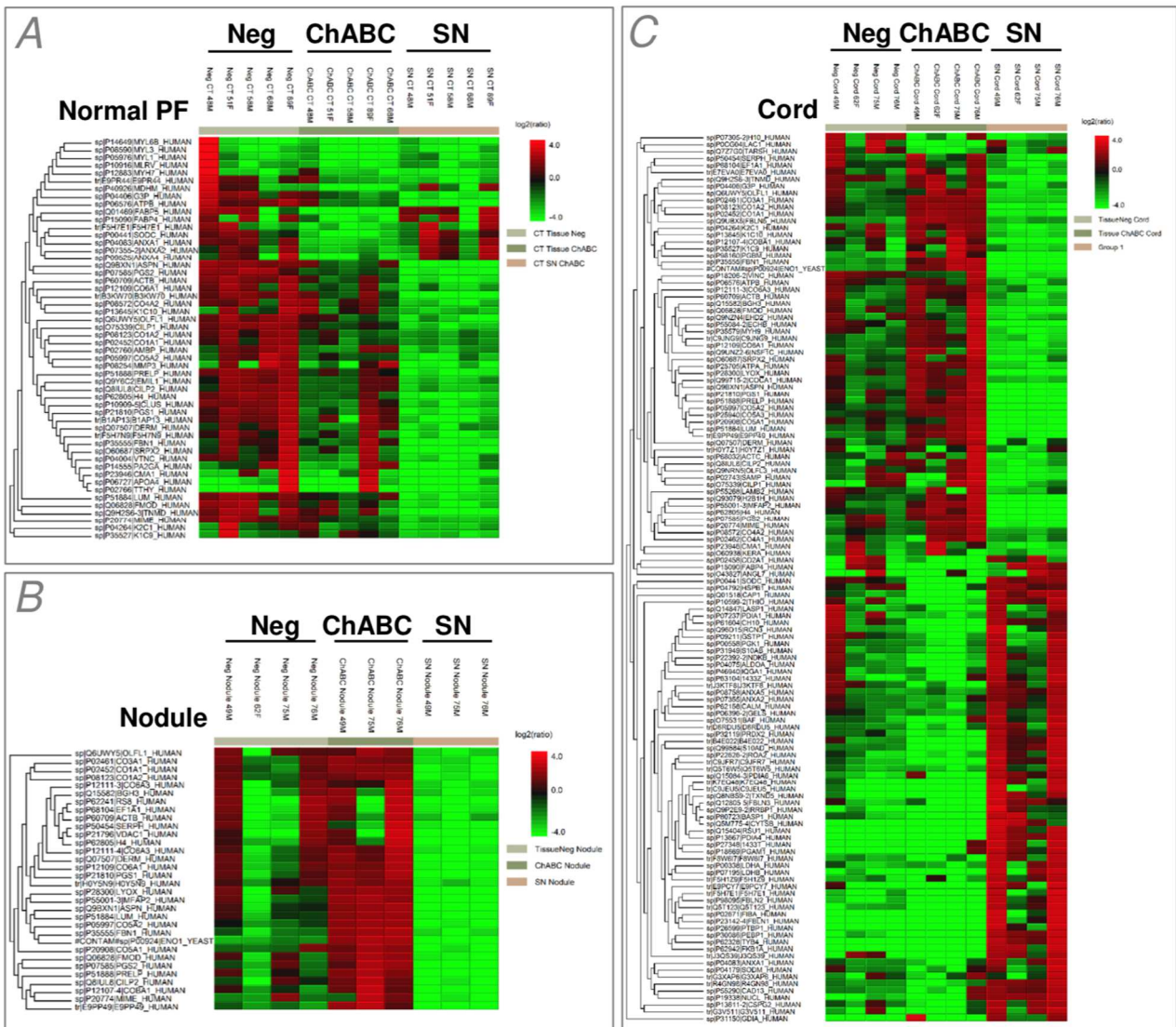
1022



1023  
1024  
1025  
1026  
1027

**Supplementary Figure S2. STRING interaction networks for normal palmar fascia (PF) and Dupuytren's explant media.** A: Interaction network for proteins enriched in normal PF explant media. B: Interaction network for proteins enriched in Dupuytren's explant media.

1028



1029

1030

1031

1032

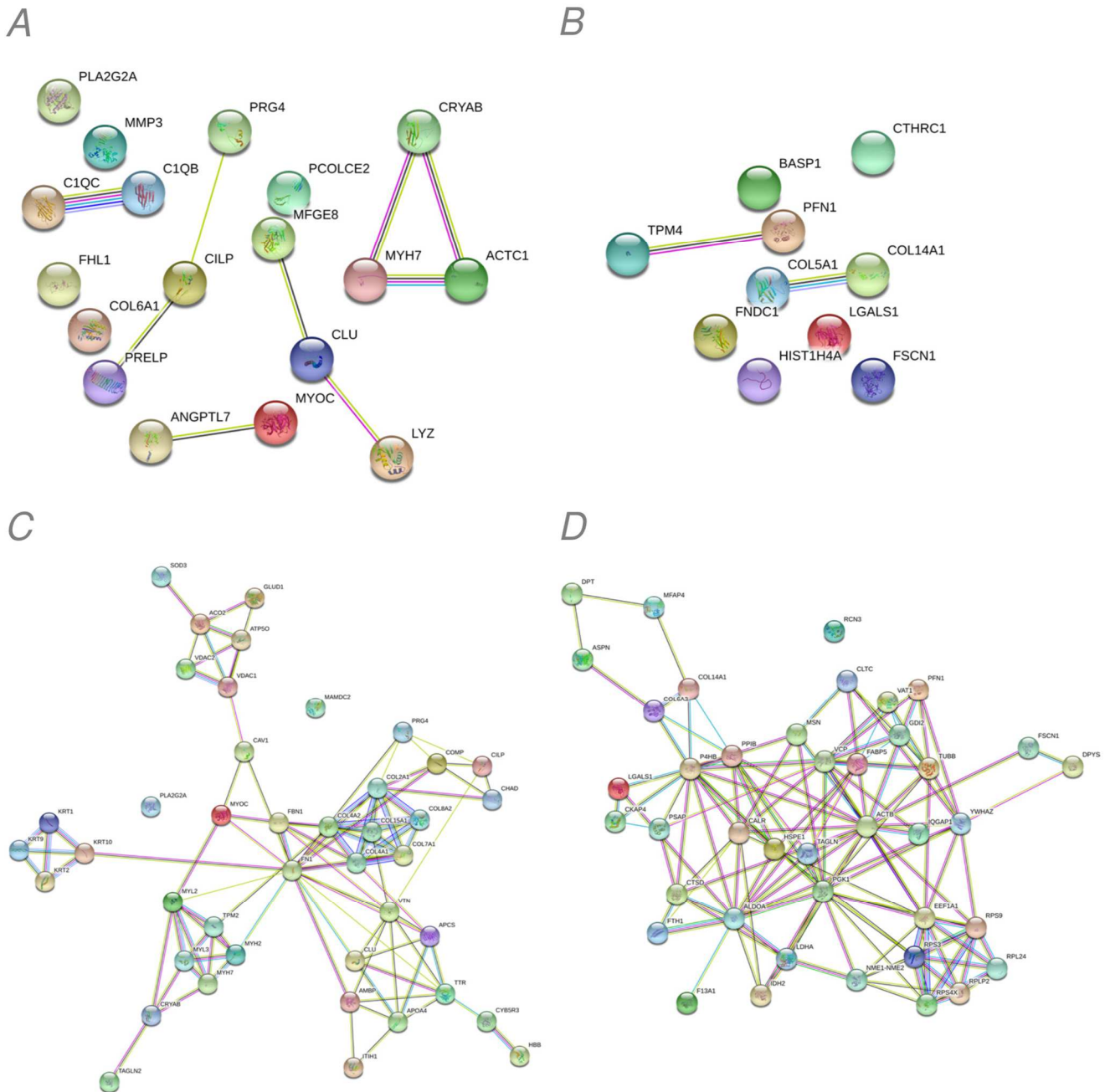
1033

1034

1035

1036

**Supplementary Figure S3. Evidence for loss of proteins into the supernatant with chondroitinase ABC treatment.** Heatmap of relative protein abundance in untreated (Neg) and chondroitinase ABC-treated (ChABC) samples as compared to the ChABC supernatant (SN) each normalised to equivalent tissue weight. A: Normal palmar fascia (PF). B: Dupuytren's nodule. C: Dupuytren's cord. The number of nodule samples was 3 rather than 4, as one ChABC -treated sample was misplaced.



1037

1038

1039

1040

1041

1042

1043

1044

1045

**Supplementary Figure S4. STRING interaction networks for normal palmar fascia (PF) and Dupuytren's explant media for proteins normalised using total ion chromatogram.** A: Interaction network for proteins enriched in normal PF explant media. B: Interaction network for proteins enriched in Dupuytren's explant media. C: Interaction network for proteins enriched in normal PF explant tissue. D: Interaction network for proteins enriched in Dupuytren's explant tissue.